ACTA INNOVATIONS

CENTRUM
BADAŃ I INNOWACJI
PRO - AKADEMIA
RESEARCH AND INNOVATION CENTRE

Ministerstwo Nauki
i Szkolnictwa Wyższego

ACTA INNOVATIONS

Contents

Paweł Leśniewicz
Institute of Turbomachinery, Lodz University of Technology
90 - 924 Łódź, 219/223 Wólczańska Street, pawel.lesniewicz@dokt.p.lodz.pl

3D PRINTING TECHNOLOGY AS A TOOL IN FABRICATION OF ELEMENTS FOR WHEEL MODEL

Abstract

This paper illustrates an experience related to the use of 3D printing technology during the fabrication of elements for a supporting arm. The arm was a part of a test stand designed for an investigation of rotating wheels in contact with the ground. One of the crucial elements of a supporting arm is the hub, which was originally made from aluminium, however it was decided to replace it by the one made from ABS using 3D printing technology. The author decided to describe difficulties encountered during fabrication of the hub, together with a set of recommendations for future use of 3D printers.

Key words
3D printing, fused deposition modelling, wheel, hub, supporting arm

Introduction

Through the year's aerodynamic analysis of vehicles was mainly focused on race cars. In construction of everyday life models aerodynamic has gained popularity since 1970s when peak oil crisis appeared. Organization of the Petroleum Exporting Countries (OPEC) proclaimed an oil embargo and prices of fuel raised. Dependency of different vehicle components on fuel consumption shows that biggest influence is connected with aerodynamic drag - 40%, the second most important factor is rolling resistance – 23% [1]. What is interesting 15% of car aerodynamic drag is connected with wheels, which is the third contributor to the aerodynamic drag [2]. To perform an investigation of rotating wheels in contact with the ground, an experimental test stand was designed and built at the Institute of Turbomachinery at Lodz University of Technology. The main elements of the stand constructed as presented in Fig.1. Road conditions were imitated by use of polyurethane belt installed on three rollers. The driving roller, connected with the motor, acts as an element responsible for delivering the movement to the belt to achieve a given linear velocity. A passive roller was located on the opposite side of the stand, and there was an additional middle roller to support the wheel model placed centrally on the belt. All three rollers were fixed together with bearings to an aluminium frame. A multi-ribbed belt transmits the power with 2:1 speed ratio from the electric motor to the active roller [3,4].
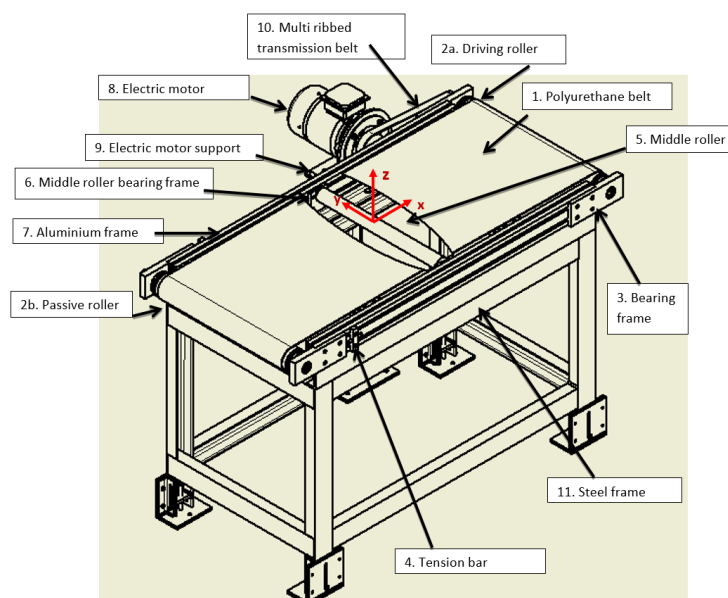
Fig. 1. Moving ground test stand
Source: [3]

Another important element of the test stand was measuring arm (see Fig.2.) responsible for preserving the position of the wheel on the belt.
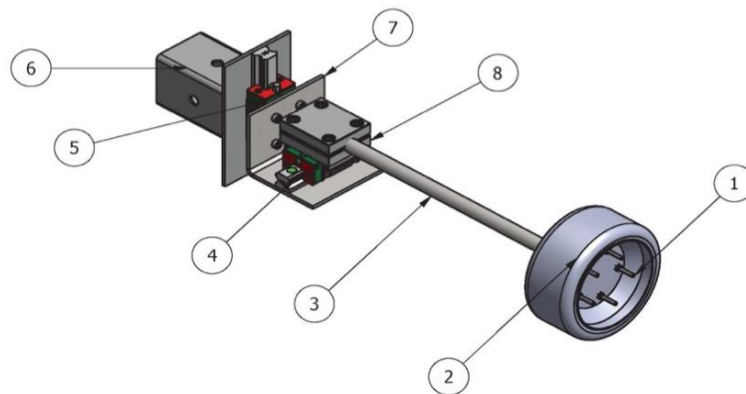
Fig. 2. Measuring arm
Source: [5]

The supporting arm consists of a rotating hub (1), a wheel model (2), an axle (3), two rails (4, 5) with a vertical (7) and horizontal (8) guideway, and a mounting sub-assembly (6) for connection to the aluminium frame. The axle is fixed and supported by two bearings. In this, construction, the wheel model rotates by means of friction transferred from the belt at the place of contact [4].

The hub was originally made from aluminium. The shape was obtained with use of lathe, then mounting holes were drilled (see Fig.3a, Fig.3b. and Fig.3c.). After the first tests, it became visible that the wheel was not centred on the axle because the mounting holes were not perfectly aligned on the hub (difference around 0.5 mm). Since the misalignment was due to human error, either a more precise way of marking and drilling should be applied, or a different way of manufacturing. The Institute offered the possibility of using 3D-printers, so it was decided to print a hub. Placing the hole with a computer eliminated human error and thereby increased the precision of the model.
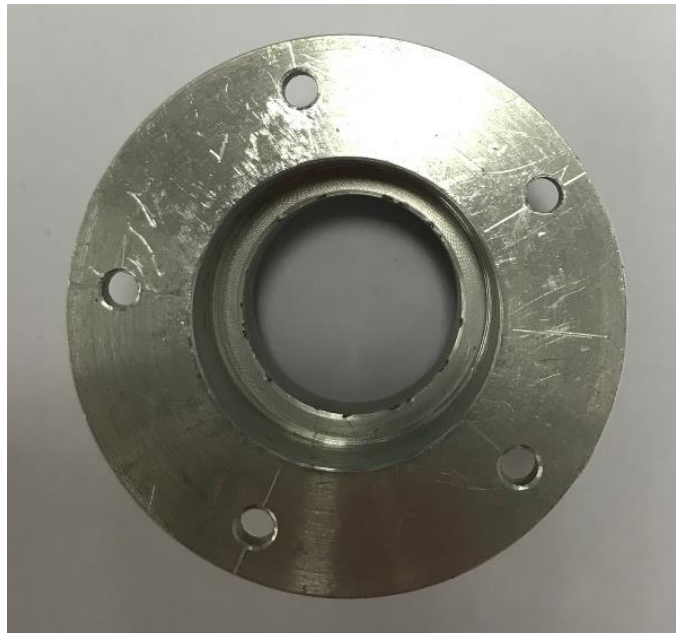
Fig. 3a. Hub made from aluminium
Source: Author's

Fig. 3b. Inner part of aluminium hub
Source: Author's
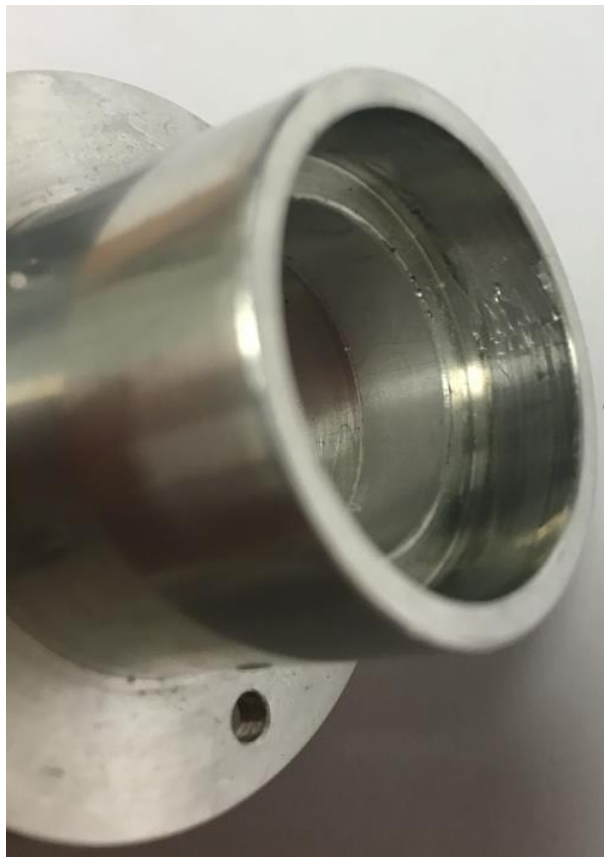
Fig. 3c. Inner part of aluminium hub
Source: Author's

Materials and methods

To create the hub, a Zortrax M200 3D printer was used (see Fig.4. for details and specification) together with Z-ABS material [6]. 3D printer that was used works in FDM (fused deposition modelling) technology which means that it prints the model with use of molten polymer imposed layer by layer [7,8]. In described work Z-ABS

material was applied as the one used by 3D printers that were accessible in the Institute (FDM printers). Selection of this material and technology was also related to its simplicity (construction of the printer, printing process), availability on the market, low price, possibility of long storage of material and treatment of printed objects. However, the author is aware that this material is relatively flexible and has high shrinkage level and some port of the problems that occurred during preparation of the hub may be related to the properties of the material itself.
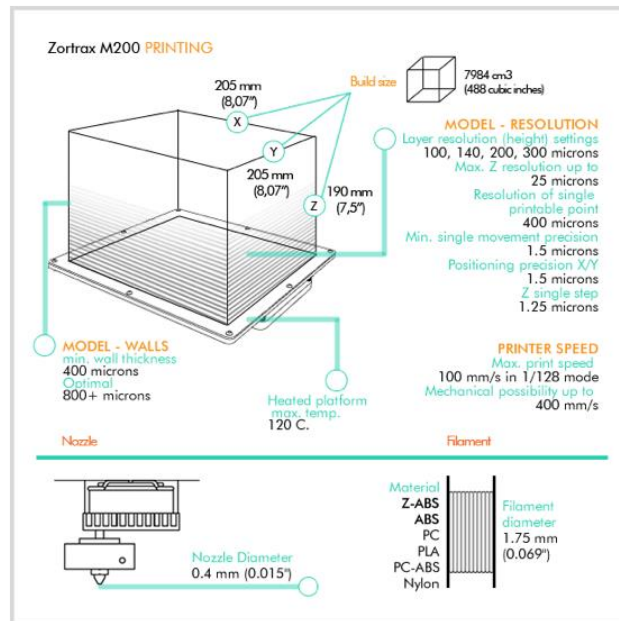
Fig. 4. Zortrax M200 3D printer
Source: [9]

A 3D CAD model of the element was created with use of Solidworks and exported to the Z-Suite software (provided by the manufacturer of the printer) to generate the code base on which printer could create the object. It is important to take into consideration resolution setup of the model during conversion to a universal file format, which is the standard file type used by rapid prototyping systems. After creating the model in a CAD software environment, it is necessary to save it as an STL (STereoLithography) file, which converts round objects into triangles. Depending on the resolution parameters, the quality of the conversion may differ [7,10,11]. That is why it is essential to select the highest possible resolution to obtain as round shape of the model as possible, remembering that the increase of resolution also increases the file size, leading to longer processing times.

At the preparation stage, the code was set to a layer thickness of 0.19 mm. Infill was selected as medium, and the angle for the supporting material as 20°. Speed and seam were marked as normal. Based on those settings, the code for the printer was generated and a simulation of the printing element was made. The set of parameters used for this simulation are presented in Table 1.

Table 1. Printer settings

Material Type	Z-ABS
Layer Thickness	0.19 mm
Quality	High
Seam	Normal
Infill	Medium
Supporting Angle	20°
Surface Layers Top	6
Surface Layers Bottom	3
Fan Speed	Auto

Source: Author's

After selecting the print settings, the Z-Suite software generated code (zcode file extension) that was used by the printer to create the object. At this stage, it was possible to check basic settings that were selected and the amount of material that was be needed to print the object. An example of that information can be found in Table 2.

Table 2. Printer settings

Profile	Z-ABS
Estimated print time	1h 16 min
Filament usage in meters	5.11 m
Filament usage in grams	12 g

Source: Author's

It was also possible to observe a simulation of the printing process. It was helpful to monitor where the supporting material was generated because after finishing the printing process that material needed to be removed. Locating the object so as to reduce the creation of supporting material in difficult to access places is advised because it can very often be problematic. Fig. 5. shows an example of a simulated printing process, where visualisations show progress in the prints at 20% intervals of completion. The main element is marked as blue, and the supporting material as grey.
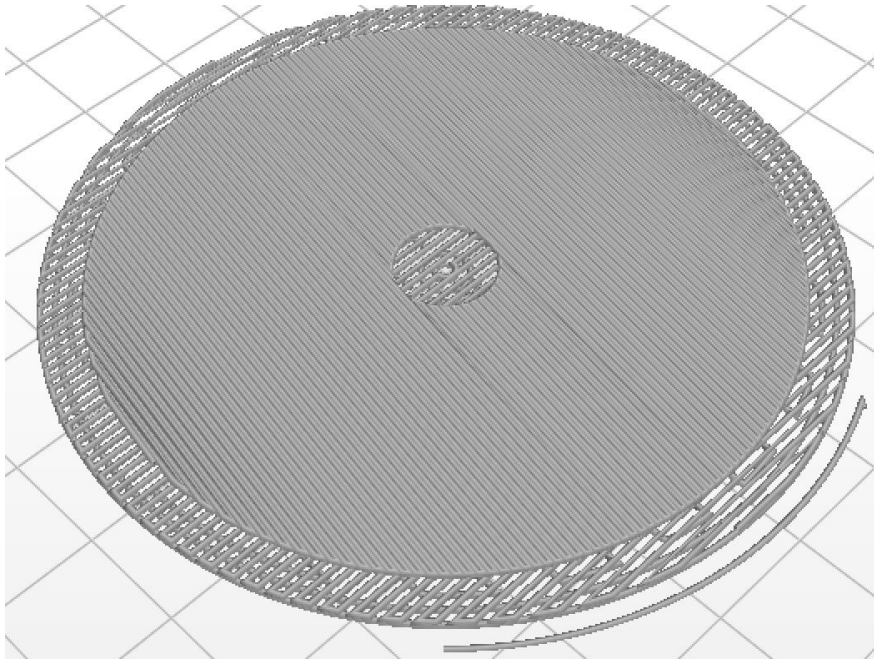
Fig. 5a. Simulation of printing process 0%
Source: Author's
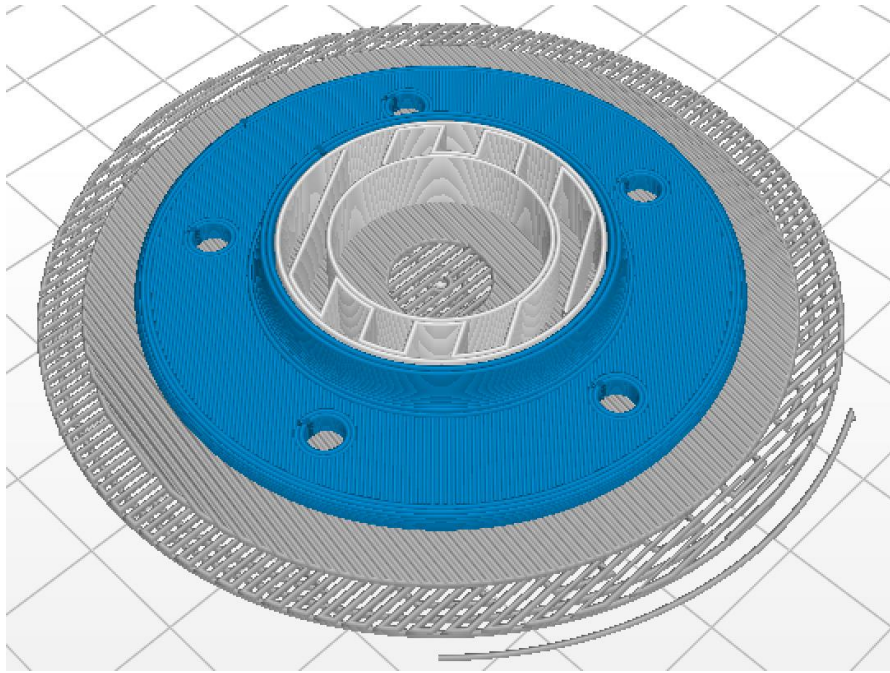
Fig. 5b. Simulation of printing process 20%
Source: Author's
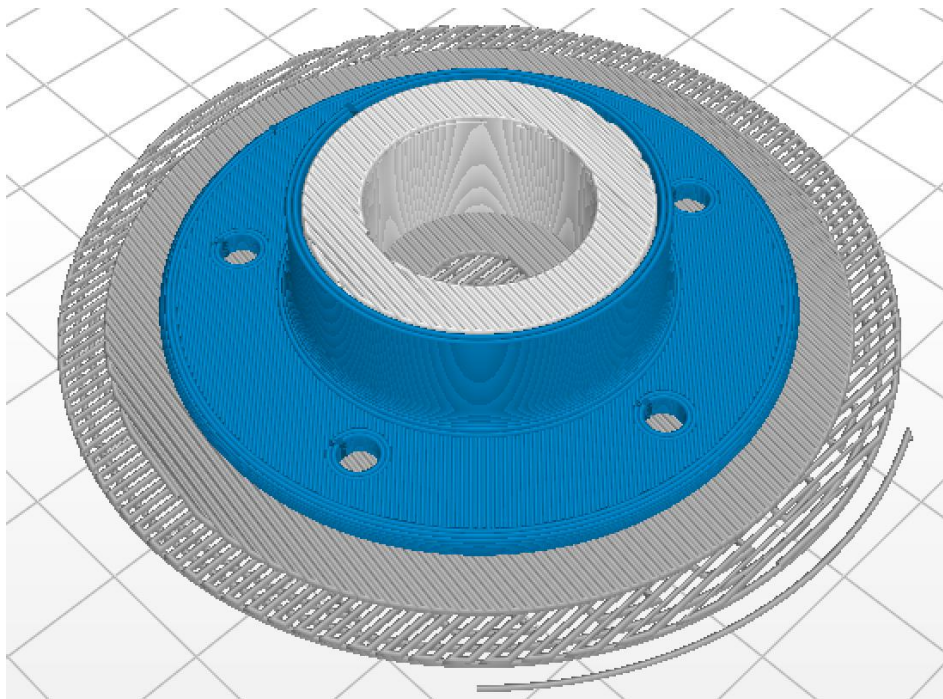
Fig. 5c. Simulation of printing process 40%
Source: Author's
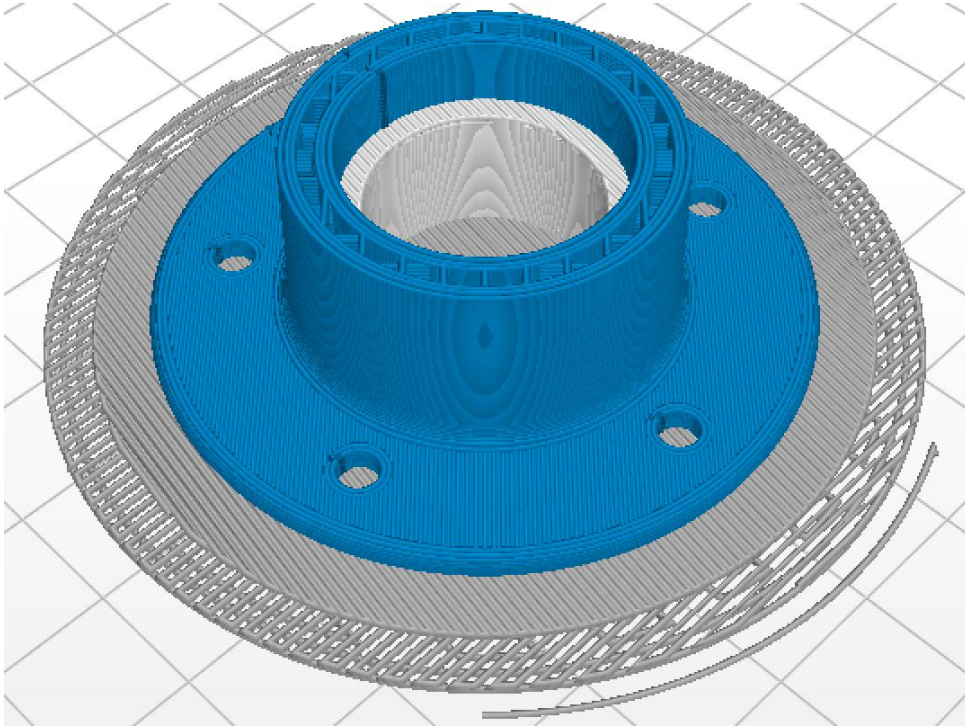
Fig. 5d. Simulation of printing process 60%
Source: Author's
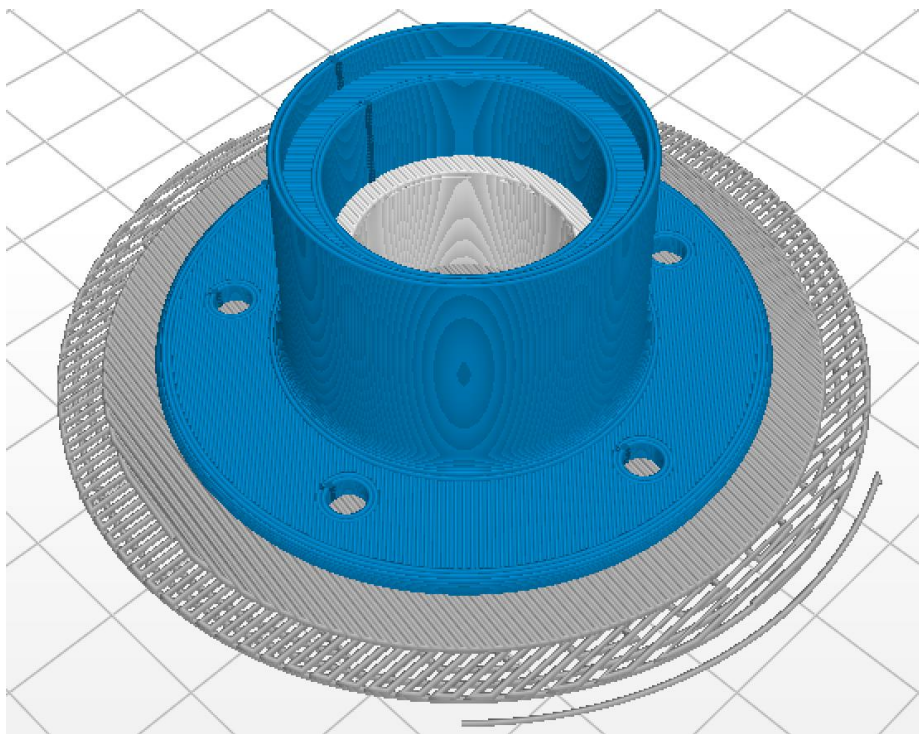
Fig. 5e. Simulation of printing process 80%
Source: Author's
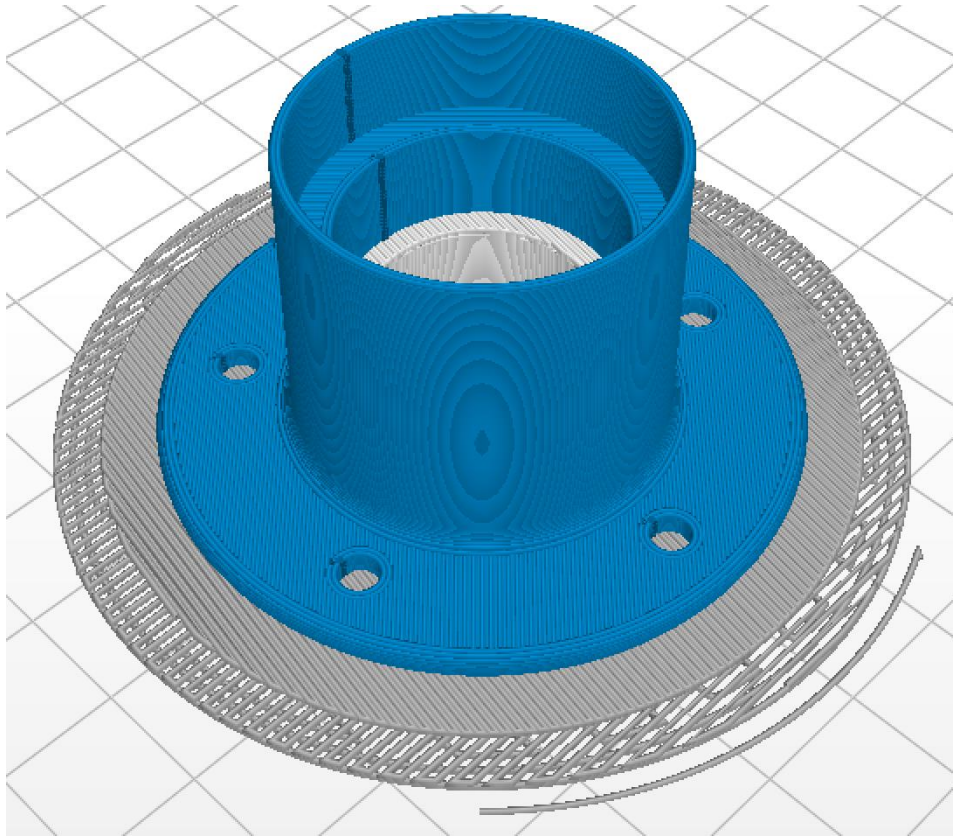
Fig. 5f. Simulation of printing process 100%
Source: Author's

Apart from the visualisation of printing process, the Z-Suite software provides information on how much material will be needed at each moment of print. Based on that it is possible to calculate at which stage printing process should be stopped if it is necessary to change the filament used for printing the model.

Results and discussion
After printing the hub, it was possible to distinguish the differences between the CAD model of the element and the result of the printing process. Although the printed hub holes diameter was equal to 2 mm, the mounting holes were designed to have a diameter of 3 mm. Due to the elastic deformation properties of the material, it was possible to use M3 screws, making it a tight fit, thereby ensuring an aligned fit of the wheel. However, there was a problem with fitting of the bearings. In the CAD model, the inner diameter of the hub was 30 mm, but the printed model had an inner diameter of 29.2 mm. Due to the previous experiences with the elastic deformation of ABS, it was decided to fit the bearings. The hub was first heated (around 70°C) to ensure that its temperature would not exceed the melting point, then the bearings were pressed in. The hub was deformed due to the excessive force needed to insert the bearings (see Fig. 6). Furthermore, during removal of the bearings from the hub, it was decomposed on to three elements, as shown in Fig. 7.
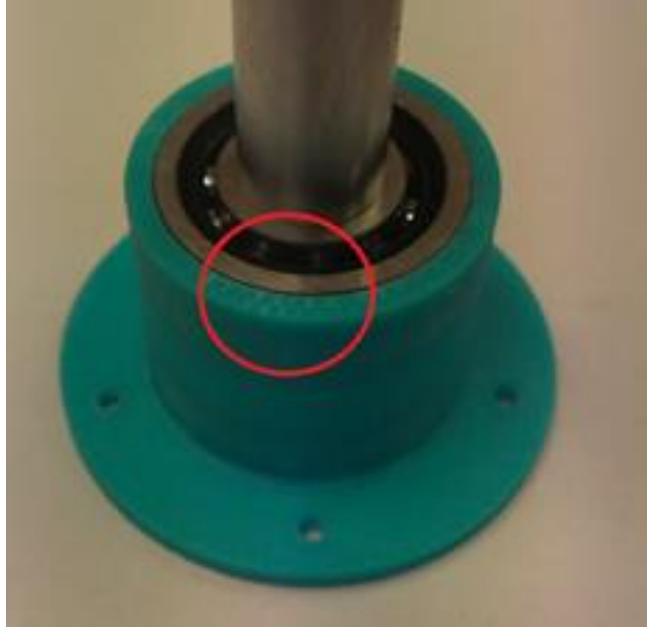
Fig. 6. Hub deformation
Source: [12]
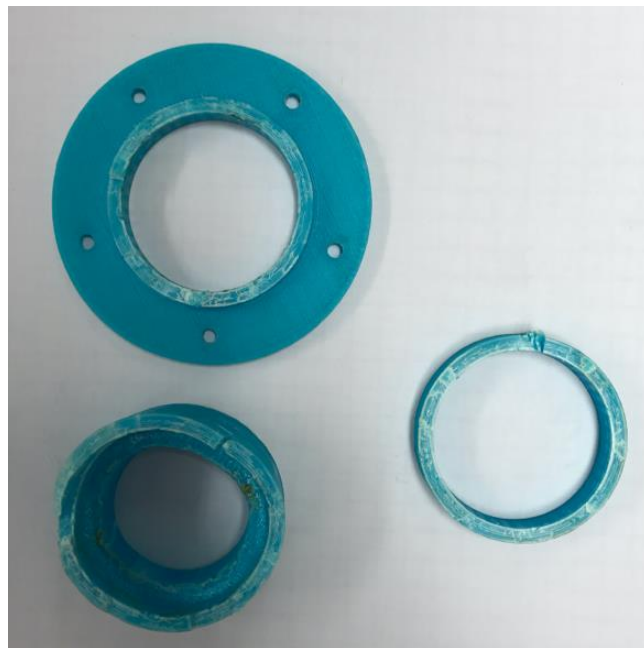
Fig. 7. Hub breakdown
Source: Author's

To eliminate the problem with the sizes of the printing holes and to find the hole size that best suits the bearing, a series of test rings were printed (see Fig. 8.). During this investigation, the programmed inner hole sizes were selected from 30 to 31 mm, with size steps of 0.2 mm. As a result of this investigation, it can be concluded that the difference with the actual sizes of the holes was linear: the actual hole size was about 0.8 mm smaller in diameter.
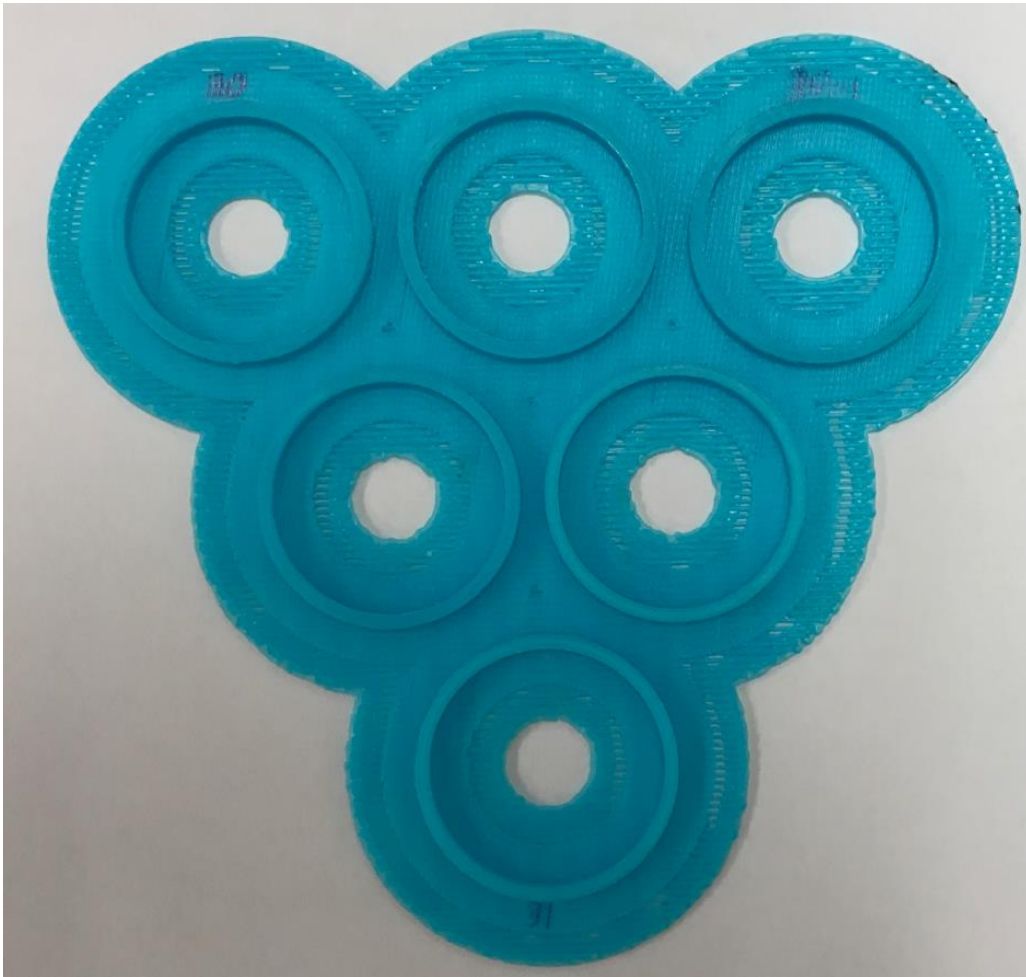
Fig. 8. Rings for hub internal diameter tests – gradually increased by 0.2mm
Source: Author's

Based on the test result presented above, it was decided to print the hub with a bearing housing size of 30.4 mm. The inner diameter of the ring between the bearings was enlarged to be able to remove the bearings more easily. The face with the mounting holes was made slightly thicker as it was deformed in the first hub. After creating the model (see Fig. 9), it can be concluded that the positioning of the bearings was perfect and the dimensions of the mounting holes were kept.
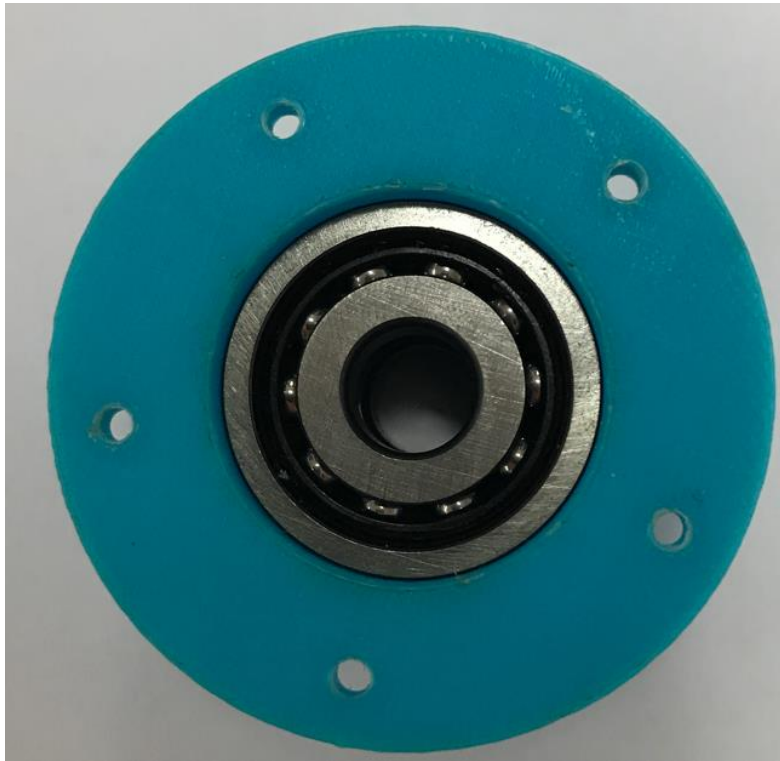
Fig. 9. Hub with bearings inside
Source: Author's

Summary
The problems described above give clear evidence that 3D printing is not an ideal solution despite the numerous advantages of this technology including possibility to create complex geometry, variety of materials, ability to influence the final shape of the object and high precision. After performing a set of tests with different hub sizes, it can be concluded that 3D printer that was used has difficulties with the creation of smooth and round elements/surfaces. The supporting material was also problematic. To print the hub, support material was added to make a bottom layer for the print, and support for the ring in the middle region of the hub. The support layers were made of the same material as the hub, and were attached to the hub more loosely than the hub material itself. Removing this material was difficult, and it may have led to the deformation of the hub when using excessive force. Also, if the surface on which the support material is attached has a rougher structure than the rest of the hub, it may need extra trimming afterwards. Part of the problems described in the above paper are common for almost all 3D printing techniques, but some port of them are limited only to the particular 3D printing technology and particular group of materials. The author is aware that polymers including ABS are relatively flexible and have high shrinkage level. Those disadvantages can be eliminated by use of SLS (Selective Laser Sintering) or SLM (Selective Laser Melting) printing techniques together with materials based on metal powders. Finally, it can be recommended to use 3D printing technology for fabrication of prototypes for preliminary and final investigations. Advantages of this manufacturing method gives a wide range of possibilities in modification of the object and selection of technique and material, however it is important to choose material and printing technology suitable for the application.

References
[1] J. Piechna, Podstawy aerodynamiki pojazdów (Basics of vehicle aerodynamics), WKŁ, Warsaw, 2000

[2] Materials from PSA Peugeot Citroën (internal use)

[3] J. Kopka, Design of an experimental stand for tests of tyre aerodynamics, BSc Diploma Thesis, Lodz University of Technology, 2014.

[4] M. Kulak et al., Numerical and experimental analysis of rotating wheel in contact with the ground, 52nd 3AF International Conference on Applied Aerodynamics, FP17-AERO2017, 2017.

[5] P. Pietrzak, Construction of the measuring arm for the experimental stand in a wind tunnel facility, BSc Diploma Thesis, Lodz University of Technology, 2016

[6] https://zortrax.com/wp-content/uploads/2015/05/Z-ABS_Material_Data_Sheet_eng-1.pdf (Z-ABS material Data Sheet, last accessed: 16.08.2017)

[7] P. Sieminski, G. Budzik, Techniki przyrostowe. Druk 3D. Drukarki 3D (Additive manufacturing, 3D printing, 3D printers), Warsaw University of Technology, Warsaw 2015

[8] L. Novakova-Marcincinova, J. Novak-Marcincin, Testing of materials for rapid prototyping fused deposition modelling technology, World Academy of Science, Engineering and Technology, vol. 6, 2012

[9] https://all3dp.com/app/uploads/2015/02/zortrax-m200-Data.png (Zortrax M200 3D printer dimensions, last accessed: 16.08.2017)

[10] B.S. Raju, U. Chanderashekar, D.N. Drakshayani, K. Chockalingam, Determining the influence of layer thickness for rapid prototyping with steroelithography (SLA) process, International Journal of Engineering Science and Technology, vol. 2, 2010

[11] K. Olasek, P. Wiklak, Application of 3D printing technology in aerodynamic study, Journal of Physics Conference Series, vol. 530, 2014

[12] B. Hoogterp, Realizing an experimental setup for the research of rotating wheel aerodynamic, BSc Diploma Thesis, Erasmus Final Project, Lodz University of Technology, 2016

Ewelina Pawlikowska, Dorota Kręgiel
Technical University of Lodz, Faculty of Biotechnology and Food Sciences, Institute of Fermentation Technology and Microbiology
Wólczańska 171/173, 90-924 Lodz, 800980@edu.p.lodz.pl

ENZYMATIC PROFILES AND ANTIMICROBIAL ACTIVITY OF THE YEAST *METSCHNIKOWIA PULCHERRIMA*

Abstract
The aim of the study was to characterize the antimicrobial properties of 5 strains belonging to the yeast species *Metschnikowia pulcherrima*. The antimicrobial activity of the strains was studied by observing pulcherrimin production and inhibition of microbial growth on YPG plates. Enzymatic assays were carried out using API ZYM tests. All strains of *M. pulcherrima* showed α-glucosidase and leucine arylamidase activities. The widest spectrum of activity was observed for strains NCYC2321, CCY145, and CCY149. All tested strains produced pucherrimin, and the yeasts *Wickerhamomyces anomalus* and *Dekkera bruxellensis*, the bacterium *Bacillus subtilis* and the moulds *Penicillium chrysogenum* and *Aspergillus brasiliensis* were the most sensitive to *M. pulcherrima*.

Key words
Metschnikowia pulcherrima, pulcherrimin, enzymatic activity, antagonism.

Introduction
As the world's population continues to grow, the global demand for food will also continue to increase. The ability to feed everyone depends upon the increase in food production and the length of storage capacity. The most popular way to prolong food usefulness is to use artificial chemicals such as pesticides. However, many of these substances are toxic to humans and are very harmful to the environment [1]. Due to the growing awareness of public opinion regarding the harmful effects to health and the environment, as well as the increasing resistance to pathogens, scientists have been interested in natural alternatives for a long time. One of these methods is the use of microorganisms that show the ability to inhibit the growth of various spoilage microorganisms, such as yeasts (*Candida* sp., *Cryptococcus* sp., *Kloeckera* sp., *Wickerhamomyces* sp., *Dekkera* sp.), bacteria (*Bacillus* sp., *Pseudomonas* sp.) or fungi (*Aspergillus* sp., *Penicillium* sp., *Fusarium* sp.) [2, 3].

The presence of spoilage microbiota may lead to significant reduction in the efficiency of any biotechnological process such as: production of wine, beer and bread, and the induction of secondary metabolite production. The interactions between various microorganisms have been described in a number of scientific studies [4, 5, 6]. The yeasts that are characterized by antagonistic activity against microbial contaminations include the genera *Pichia, Candida, Aureobasidium, Metschnikowia*, and *Debaryomyces*. The presence of microbial contamination not only reduces nutrients availability for industrial microorganisms, but also reduces environmental succession [7]. The low nutrient availability is one of the most important mechanisms of competition between microbial strains. However, the antagonistic properties of yeasts can also be attributed to the changes in the pH values elicited by the production of organic acids, production and tolerance to high concentrations of ethanol, and the secretion of extracellular antimicrobial compounds, for example, killer toxins or enzymes [2, 8].

The yeasts *Metchnikowia* spp. are very interesting microbial models because they occur as members of the natural microbiota of flowers, fruits and insects [9]. The antagonistic properties of these yeasts have been described in the literature [10, 11, 12, 13], and especially *M. pulcherrima* strains show a great potential to become efficient biological control agents of natural origin against a broad spectrum of saprophytic and pathogenic microorganisms. It is well-documented [8, 14, 15] that *Metschnikowia* spp. are antagonistic to various fungi and bacteria. The possible mechanisms of action involved in the antagonistic activities of those yeasts are: (a) antibiosis, whereby the yeast cells produce antimicrobial compounds, (b) competition, when habitat or nutrients (i.e. source of carbon, nitrogen, as well as microelements) are limiting factors, (c) other mechanisms, *e.g.* by which *Metchnikowia* spp. attack other microbial cells including the secretion of lytic

enzymes (proteases, glucanases and chitinases) that enable them to degrade the cells and utilize their biopolymers as nutrients [8, 14].

The inhibitory activities of *M. pulcherrima* strains have been confirmed mainly for moulds: *e.g. Penicillium* spp., *Alternaria* spp., *Aspergillus* spp., *Fusarium* spp. and *Botrytis cinerea* [14, 15, 16]. It has been also demonstrated that *M. pulcherrima* showed antimicrobial activity against numerous yeasts belonging to the genera *Pichia*, *Candida*, *Hanseniaspora*, *Kluyveromyces*, *Saccharomycodes*, *Torulaspora* and *Brettanomyces* [12]. Interestingly, the antimicrobial activity of *M. pulcherrima* did not affect the growth of *Saccharomyces cerevisiae* at all [17]. It has been shown that the antimicrobial activity of *M. pulcherrima* depends on the formation of pulcherrimin [18] and, therefore, strains that produce large amounts of pulcherrimic acid are of great interest to scientists, and can be considered as potential natural agents to control the growth of the spoilage microbiota [11, 19].

The aim of this study was to investigate the enzyme productions of 5 strains belonging to *M. pulcherrima*, which were obtained from two European collections – the National Collection of Yeast Cultures (NCYC, UK) and the Culture Collection of Yeasts (CCY, Slovakia). Enzyme assays were carried out using a commercial API ZYM test (bioMérieux). In addition, the antimicrobial activity of the yeast strains was studied by estimating (1) pulcherrimin production *via* the formation of pulcherrimin acid and Fe^{3+} complexes, as well as (2) inhibition of microbial (yeasts, bacteria, moulds) growths on YPG plates.

Materials and methods
Microorganisms
All mould and yeast strains were grown on YPG agar at 25°C. Bacterial strains of *Bacillus* sp. and *Pseudomonas* sp. were cultivated on nutrient agar at 30-37°C. Acetic acid bacterium belonging to *Asaia* sp. were cultivated on GC agar at 25°C [20].

The microorganisms tested in this study are presented in Table 1. These strains were isolated as members of spoilage microbiota present in different food products.

Table 1. The microorganisms used in the study.

Group	Name	Origin
Yeasts	*Metschnikowia pulcherrima* CCY145	The Culture Collection of Yeasts (Slovakia)
	Metschnikowia pulcherrima CCY147	
	Metschnikowia pulcherrima CCY149	
	Metschnikowia pulcherrima NCYC2321	National Collection of Yeast Cultures (UK)
	Metschnikowia pulcherrima NCYC747	
	Wickerhamomyces anomalus C1	Isolated as a spoilage yeast of soft drinks [21]
	Dekkera bruxellensis C2	
Bacteria	*Bacillus subtilis* LOCK0816	Collection of Industrial Microorganisms LOCK 105 (Poland)
	Pseudomonas aeruginosa LOCK0885	
	Asaia bogorensis ISD1	Isolated as a spoilage bacterium of soft drinks [22]
Moulds	*Penicillium chrysogenum* LOCK0531	Collection of Industrial Microorganisms LOCK 105 (Poland)
	Aspergillus brasiliensis LOCK0436	

Source: Author's

Testing pulcherrimin production
To compare the pigment productions by *M. pulcherrima* colonies growing on agar plates, yeast cells were streaked on YPG agar plates supplemented with $FeCl_3$ (0.015mg/ml), and the widths of the reddish halos around the yeast colonies were observed after 5 days of incubation at 25°C [23].

Testing antagonism
For antagonistic activity tests, 200µL aliquots of each yeast, bacterium and mould suspensions (4°McF) was spread evenly on YPG agar plates. When the surface of plates dried, *M. pulcherrimin* cells were streaked on agar plates, and then the plates were incubated at 25°C for 2-5 days due to the various growth rates of the

bacterium, yeast and mould strains (Table 1). The antagonism was quantified by the diameters of the zones of no growth around the *M. pulcherrima* CCY145 culture (mm) [12, 23].

Enzyme assays
The soluble enzyme activity in yeasts suspension samples was determined by the API ZYM kit (bioMérieux), which is commercially available for the semi-quantitative analysis of hydrolytic enzyme production. Each strip is composed of 20 microwells containing dehydrated chromogenic substrates for 19 enzymatic reactions and a control. Microwells contain a buffer with a specific optimum pH value for each enzyme activity. Yeast cell suspensions (5-6°McF; 65 µl aliquots) were dispensed into the 20 microwells. Sterile water was added into a plastic outer cover to create a humidity chamber. The API ZYM strips were covered and incubated at 37°C for 4 h according to the instructions provided by the manufacturer. After that, one-one drops (30 µl each) of the commercial reagents ZYM A and ZYM B (bioMérieux) were added to all microwells to develop the colours of the reaction mixtures. The colour reactions were read after 5 minutes, and a digit ranging from 0 to 5 was assigned to each sample following the colour chart provided by the manufacturer.

Results
Enzyme activities of the yeast *Metschnikowia pulcherrima*
Enzyme activities of the tested yeast strains are presented in Table 2.

Table 2. Enzyme activities of *M. pulcherrima* strains

Enzyme→ Strain ↓	1	2	3	4	5	6	7	8	9	10	11	12	13	14	15	16	17	18	19	20
NCYC 2321	0	0	3	2	0	4	1	0	0	0	3	3	0	0	0	5	2	0	0	0
NCYC 747	0	0	2	2	0	4	1	0	0	0	1	3	0	0	0	5	2	0	0	0
CCY 145	0	0	2	1	0	4	1	0	1	0	3	4	0	0	0	4	0	0	0	0
CCY 147	0	0	1	1	0	4	0	0	0	0	2	2	0	0	0	5	1	0	0	0
CCY 149	0	2	3	3	0	3	1	0	0	0	1	2	0	0	0	5	2	0	0	0

1: Control, 2: Alkaline phosphatase, 3: Esterase (C4), 4: Esterase lipase (C8), 5: Lipase (C14), 6: Leucine arylamidase, 7: Valine arylamidase, 8: Cystine arylamidase, 9: Trypsin, 10: α-chymotrypsin, 11: Acid phosphatase, 12: Naphtol-AS-BI-phosphohydrolase, 13: α-galactosidase, 14: β- galactosidase, 15: β-glucuronidase, 16: α-glucosidase, 17: β-glucosidase, 18: N-acetyl-β-glucoaminidase, 19: α-mannosidase, 20: α-fucosidase
Source: Author's

All tested *M. pulcherrima* strains were characterized by high α-glucosidase (value 4-5) and leucine arylamidase activities (value 3-4). Some of the tested strains also showed significant esterase (C4), esterase lipase, acid phosphatase, naphtol-AS-BI-phosphohydrolase and β-glucosidase activities. The widest spectrum of hydrolytic enzyme activities was observed with the strains NCYC2321, CCY145, and CCY149.

Pulcherrimin production
All tested strains of *M. pulcherrima* formed reddish pigment on YPG medium when supplemented with Fe^{3+} ions (Figure 1).

Fig. 1. Production of red pigment by the tested *Metschnikowia pulcherrima* strains in YPG agar medium supplemented with Fe^{3+} ions (0,015mg/ml). A *Wickerhamomyces anomalus* strain without pigment production was used as negative control.
Source: Author's

Inhibition of microbial growth

All tested *Metschnikowia* strains inhibited the growth of the Gram-positive bacterium *Bacillus subtilis*, the yeasts *Dekkera bruxellensis* and *Wickerhamomyces anomalus*, and the moulds *Penicillium chrysogenum* and *Aspergillus brasiliensis* (Figure 2). The widths of growth inhibition zones noted around the tested *M. pulcherrima* strains varied by the tested species (Table 3). In the case of the bacterium *Pseudomonas aeruginosa* and *Asaia bogorensis* no inhibitory effects of *M. pulcherrima* were observed.

Table 3. Inhibition of microbial growth by *M. pulcherrima* CCY145

Microorganisms tested	Zone of inhibition after 48-120 h incubation (mm)
Wickerhamomyces anomalus	7
Dekkera bruxellensis	4
Bacillus subtilis LOCK0816	4
Pseudomonas aeruginosa LOCK0885	0
Asaia bogorensis ISD1	0
Penicillium chrysogenum LOCK0531	3
Aspergillus brasiliensis LOCK0436	1

Inhibition zones were measured as the distance from the edge of *M. pulcherrima* colonies to the beginning of the microorganism colonies on YPG agar plates at 48-120 h of incubation depending on the species.
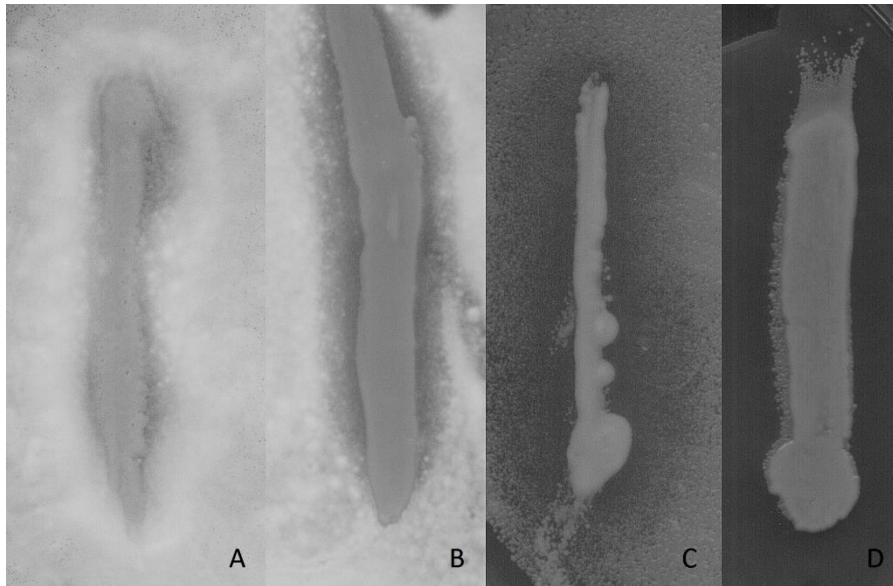*Source: Author's*

Fig. 2. The inhibition of microbial growths by a *M. pulcherrima* strain (CCY147) as shown by the dark zones of no growth around the yeast colonies. A - *Aspergillus brasiliensis*, B – *Penicillium chrysogenum*, C - *Wickerhamomyces anomalus*, D - *Bacillus subtilis*.
Source: Author's

Discussion

In industrialized countries, organic agriculture is based on clearly defined natural methods, and this offers many environmental benefits to the users. Artificial pesticides can pollute groundwater, disrupt key ecological processes such as pollination, threaten beneficial microorganisms, and represent serious health hazards to humans. In contrast, organic agriculture sets out to enhance biodiversity and restore the natural ecological balance. It encourages both spatial and temporal biodiversity through intercropping and crop rotations, conserves soil and water resources, and builds soil organic matter and biological processes. Livestock and diseases are kept at bay by crop associations, symbiotic combinations, and other nonchemical methods. In this context, the possibility of application of the antagonistic yeasts against undesirable spoilage microorganisms is the subject of interest for both scientists and technologists [1, 24].

The biological control of plant pathogens with antagonistic microorganisms is an efficient alternative to synthetic fungicides in reducing postharvest diseases and product loss. Yeasts are considered among the most promising antagonists in such biocontrol strategies [25]. Some of these microorganisms with Generally Recognized As Safe (GRAS) status and without special nutrient requirements can colonize both surfaces of fruits and vegetables. They are resistant to temperature changes, dryness, and sunlight [8], and are cheap for both small scale and large scale productions [26].

It is known that strains of the yeast *M. pulcherrima* have a great potential to become a leading natural and biological control agent against a broad spectrum of spoilage microorganisms [14]. In addition, *Metschnikowia* spp. with a wide temperature tolerance do not produce either allergic spores or harmful mycotoxins, thus they can be included in commercial preparations to protect fruits and vegetables both before and after harvesting [8].

In the literature, the researchers pointed to the possibility of the production of killer toxins by *M. pulcherrima* [27, 28], however those reports have been verified, current results indicated that the antibacterial activities of *M. pulcherrima* are associated with changes in the extracellular pH values and not with the biosynthesis of killer toxins. In the case of yeasts and moulds, the antagonism with *M. pulcherrima* is attributed to pulcherrimic acid secretion, which accumulates in the growth medium. This organic acid captures Fe^{3+} ions that are required for the proper growths of spoilage microorganisms. In fact, the production of acidic compounds (including pulcherrimic acid) decreases the pH of the environment and, as a result, the acidic pH together with the extraction of iron can inhibit the growth of other microbial cells [12]. Not surprisingly, recent publications in

this field suggest that the antibacterial and antifungal activities of the yeast *M. pulcherrima* depend clearly on pulcherrimin production [14, 29].

As expected, the *M. pulcherrima* strains tested in this study effectively inhibited the growths of various spoilage microorganisms, including various moulds (*P. chrysogenum, A. brasiliensis*), yeasts (*D. bruxellensis, W. anomalus*) and also the bacterium *B. subtilis*. These microorganisms often spoil agroproducts, food, and fermentation products [3, 23, 30]. Interestingly, studies conducted by Csutak et al. suggested that wild-type strains of *M. pulcherrima*, isolated directly from fruit microbiota, exhibited higher antagonistic activity when compared to those of the strains bought from culture collections. This observation may be the consequence of the adaptation of the strains to the maintenance and growth conditions employed in the strain collections [10].

The tested *M. pulcherrima* strains showed antagonistic activity against the yeast strains belonging to *W. anomalus* and *D. bruxellensis,* probably owing to their Fe^{3+} binding capabilities. Obviously, satisfactory iron supplementation is necessary for the proper growth of wild-type yeasts. According to pervious literature data [31, 32], *W. anomalus* can grow under extreme environmental stress conditions, *e.g.* at low and high pH values, low water activity, high osmotic pressure and also under anaerobic conditions. As a consequence, *W. anomalus* is a common member of the spoilage microbiota, *e.g.* in fruits and high-sugar food products [32]. *D. bruxellensis* is a common spoilage yeast too, occurring in fermented products. This yeast tolerates well high ethanol concentration, low pH value, and nitrogen starvation. *D. bruxellensis* is a facultative anaerobic yeast, which may be predominant under environmental conditions unfavourable for other microorganism [33]. *M. pulcherrima* has been showed to possess antimicrobial activity against a wide spectrum of yeasts. For example, Oro et al. demonstrated the antimicrobial activity of *M. pulcherrima* against *Pichia* spp., *Candida* spp. and *Brettanomyces* spp. [12].

All tested strains of *M. pulcherrima* inhibited the growth of the Gram-positive bacterium *B. subtilis*. This bacterium belongs to the typical spoilage microbiota observed in various environments, including fruits, vegetables or even fermentation media [3, 34, 35]. Inhibitory effect of *M. pulcherrima* was also recorded for the moulds *P. chrysogenum* and *A. brasiliensis* [14]. These moulds are highly aerobic and they are found in almost all oxygen-rich environments [36]. Generally, these fungi grow on carbon-rich substrates like monosaccharides (glucose) and polysaccharides (starch) and, therefore, these species are common contaminants on foods [37]. Members of these genera possess the ability to grow under high osmolarity (high sugar, salt, etc.) conditions [38]. Black aspergilli are widespread in vineyards, cause rots on berries, and are also the main sources of ochratoxin A contaminations [25].

Our experimental data demonstrated that the tested strains of *M. pulcherrima* were able to produce different hydrolytic enzymes, and these enzyme activities may be useful in biocontrol processes. The available literature shows that these strains can secrete lytic enzymes, which hydrolyze a variety of polymeric compounds (chitin, proteins) [14].

Conclusions

In our study, we recorded a broad spectrum of antibacterial and antifungal activities for the yeast *M. pulcherrima*. The data presented here demonstrated a high potential for some *M. pulcherrima* strains to become biocontrol agents, which can be employed in various environments against many spoilage bacteria, yeasts and moulds.

References

[1] F.P. Carvalho, Agriculture, pesticides, food security and food safety, Environ. Sci. Policy. 9 (2006) 685–692.

[2] D. Spadaro, R. Vola, S. Piano, M.L. Gullino, Mechanisms of action and efficacy of four isolates of the yeast *Metschnikowia pulcherrima* active against postharvest pathogens on apples, Postharvest Biol. Tec. 24 (2002) 123–134.

[3] R.R. Sharma, D. Singh, R. Singh, Biological control of postharvest diseases of fruits and vegetables by microbial antagonists: A review, Biol. Control. 50 (2009) 205–221.

[4] P. Frey-Klett, P. Burlinson, A. Deveau, M. Barret, M. Tarkka, A. Sarniguet, Bacterial-fungal interactions: hyphens between agricultural, clinical, environmental, and food microbiologists, Microbiol. Mol. Biol. R. 75 (2011) 583–609.

[5] W.I. Golubev, Antagonistic interactions among yeasts, w: G. Péter, C. Rosa (Eds.), Biodiversity and ecophysiology of yeasts., Springer-Verlag, Berlin/Heidelberg, 2006, ss. 197–221.

[6] D. Spadaro, S. Droby, Development of biocontrol products for postharvest diseases of fruit: The importance of elucidating the mechanisms of action of yeast antagonists, Trends Food Sci. Tech. 47 (2016) 39–49.

[7] M. Grzegorczyk, A. Szalewicz, B. Żarowska, X. Połomska, W. Wątorek, M. Wojtatowicz, Drobnoustroje w biologicznej ochronie roślin przed chorobami grzybowymi, Acta Sci. Pol., Biotechnol. 14 (2015) 19–42.

[8] S. Muccilli, C. Restuccia, Bioprotective role of yeasts, Microorganisms. 3 (2015) 588–611.

[9] L.C. Mendonca-Hagler, A.N. Hagler, C.P. Kurtzman, Phylogeny of *Metschnikowia* species estimated from partial rRNA sequences, Int. J. Syst. Bacteriol. 43 (1993) 368–373.

[10] O. Csutak, I. Sarbu, T. Vassu, Influence of sodium bicarbonate, calcium chloride and growth media on antimicrobial activity of *Metschnikowia pulcherrima*, J. Food Sci. Eng. 3 (2013) 79–86.

[11] S. Türkel, B. Ener, Isolation and characterization of new *Metschnikowia pulcherrima* strains as producers of the antimicrobial pigment pulcherrimin, Z. Naturforsch. C. 64 (2009) 405–410.

[12] L. Oro, M. Ciani, F. Comitini, Antimicrobial activity of *Metschnikowia pulcherrima* on wine yeasts, J. Appl. Microbiol. 116 (2014) 1209–1217.

[13] E. de Curtis, E.S. Torriani, E. Rossi, V. de Cicco, Selection and use of *Metschnikowia pulcherrima* as a biological control agent for postharvest rots of peaches and table grapes, Ann. Microbiol. Enzym.. 46 (1996) 45–55.

[14] S. Türkel, M. Korukluoğlu, M. Yavuz, Biocontrol activity of the local strain of *Metschnikowia pulcherrima* on different postharvest pathogens, Biotechnol. Res. Int. 2014 (2014) 397167.

[15] D. Saravanakumar, A. Ciavorella, D. Spadaro, A. Garibaldi, M.L. Gullino, *Metschnikowia pulcherrima* strain MACH1 outcompetes *Botrytis cinerea, Alternaria alternata* and *Penicillium expansum* in apples through iron depletion, Postharvest Biol. Tec. 49 (2008) 121–128.

[16] W.J. Janisiewicz, T.J. Tworkoski, C.P. Kurtzman, Biocontrol potential of *Metchnikowia pulcherrima* strains against blue mold of apple, Phytopathology. 91 (2001) 1098–1108.

[17] F. Comitini, M. Gobbi, P. Domizio, C. Romani, L. Lencioni, I. Mannazzu, M. Ciani, Selected non-*Saccharomyces* wine yeasts in controlled multistarter fermentations with *Saccharomyces cerevisiae*, Food Microbiol. 28 (2011) 873–882.

[18] A. Espinel-Ingroff, Mechanisms of resistance to antifungal agents: yeasts and filamentous fungi, Rev. Iberoam. Micol. 25 (2008) 101–106.

[19] I.C. MacWilliam, A survey of the antibiotic powers of yeasts, J. Gen. Microbiol. 21 (1959) 410–414.

[20] D. Kregiel, A. Otlewska, H. Antolak, Attachment of *Asaia bogorensis* originating in fruit-flavored water to packaging materials, Biomed Res. Int. 2014 (2014) 514190.

[21] M. Dudkiewicz, J. Berlowska, D. Kregiel, Acid whey as a medium for cultivation of conventional and non-conventional yeasts, Biotechnol. Food Sci. 80 (2016) 75-82

[22] H. Antolak, A. Czyżowska, D. Kregiel, Black Currant (*Ribes nigrum* L.) and Bilberry (*Vaccinium myrtillus* L.) fruit juices inhibit adhesion of *Asaia* spp., Biomed Res. Int. 2016 (2016) 3671306

[23] M. Sipiczki, *Metschnikowia* strains isolated from botrytized grapes antagonize fungal and bacterial growth by iron depletion, Appl. Environ. Microbiol. 72 (2006) 6716–6724.

[24] G. Rundgren, Organic agriculture and food security. Dossier, IFOAM, Germany, 2006.

[25] S. Fiori, P.P. Urgeghe, W. Hammami, S. Razzu, S. Jaoua, Q. Migheli, Biocontrol activity of four non- and low-fermenting yeast strains against *Aspergillus carbonarius* and their ability to remove ochratoxin A from grape juice, Int. J. Food Microbiol. 189 (2014) 45–50.

[26] R.S. Pimenta, P.B. Morais, C.A. Rosa, A. Corrêa, Utilization of yeasts in biological control programs, w: T. Satyanarayana, G. Kunze (Eds.), Yeast biotechnology: diversity and applications, Springer, Netherlands, 2009, ss. 199–214.

[27] G.A. Farris, I. Mannazzu, M. Budroni, Identification of killer factor in the yeast genus *Metschnikowia*, Biotechnol. Lett. 13 (1991) 297–298.

[28] C.A. Lopes, M.P. Sangorrin, Optimization of killer assays for yeast selection protocols, Rev. Argent. Microbiol. 42 (2010) 298–306.

[29] A.J. Kluyver, J.P. van der Walt, A.J. van Triet, Pulcherrimin, the pigment of *Candida pulcherrima*, P. Natl. Acad. Sci. USA. 39 (1953) 583–593.

[30] N.P. Jolly, C. Varela, I.S. Pretorius, Not your ordinary yeast: non-*Saccharomyces* yeasts in wine production uncovered, FEMS Yeast Res. 14 (2014) 215–237.

[31] E. Fredlund, U. Druvefors, M. E. Boysen, K.-J. Lingsten, J. Schnürer, Physiological characteristics of the biocontrol yeast *Pichia anomala* J121, FEMS Yeasts Res. 2 (2002) 395-402.
[32] P. Satora, T. Tarko, P. Sroka, U. Blaszczyk, The influence of *Wickerhamomyces anomalus* killer yeast on the fermentation and chemical composition of apple wines, FEMS Yeast Res. 14 (2014) 729–740.

[33] A.J. Schifferdecker, S. Dashko, O.P. Ishchuk, J. Piškur, The wine and beer yeast *Dekkera bruxellensis*, Yeast, 31 (2014) 323–332.

[34] A. Barata, M. Malfeito-Ferreira, V. Loureiro, The microbial ecology of wine grape berries, Int. J. Food Microbiol. 153 (2012) 243–259.

[35] K.R. Aneja, R. Dhiman, N.K. Aggarwal, V. Kumar, M. Kaur, Microbes associated with freshly prepared juices of citrus and carrots," Int. J. Food Sci. 2014 (2014) 1–7.

[36] S.A. Bolu, N. Elelu, R.N. Ahmed, F.E. Solaojo, K.F. Daramola, V.S. Omotosho, A.G. Atitebi, M. Afeni, Effect of vitamins, amino acids and phyto-active biomolecules on *Aspergillus flavus* in poultry production, w: S.J.T. Gowder (Eds.), Pharmacology and Therapeutics, 2014, ss. 23-45.

[37] F. Bosco, C. Mollea, Mycotoxinns in food, w: B. Valdez (Eds.), Food Industrial Processes – Methods and equipment, InTech, 2012, ss. 169-200.

[38] J. Houbraken, R.P. de Vries, R.A. Samson, Moder taxonomy of biotechnologically important *Aspergillus* and *Penicillium* species, Adv. Appl. Micriobiol. 86 (2014) 199-249.

Łukasz Przybysz, Mariola Błaszczyk, Jerzy Sęk
Lodz University of Technology, Faculty of Process and Environmental Engineering, Department of Chemical Engineering
213 Wolczanska St., 90-924 Lodz, Poland, luk.przybysz@o2.pl, mar.blaszczyk@o2.pl, jerzysek@p.lodz.pl

INFLUENCE OF EMULSION INNER PHASE CONCENTRATION ON PERMEABILITY OF DEPOSIT DURING FLOW THROUGH POROUS MEDIA

Abstract
The issue of emulsion flow through porous media plays an important role in the development of land purification methods from various oily substances, as well as during the oil extraction process. The concentration of the emulsion dispersed phase exerts a strong influence on the rheological properties. The oil in water emulsions (O/W), that have a concentration of less than 0.5 (or 50%), show Newtonian behavior, and those with higher concentrations non-Newtonian. The flow of such systems through the structure of the porous medium is, therefore, also dependent on the variable rheological properties of the liquid. When the emulsion flows through the porous medium, a reduction of the relative permeability occurs. Due to that the transport may be very effectively limited, as the pores of deposit are being blocked by oil droplets. The paper presents studies on emulsion flow, with various concentrations, through a granular bed. It allowed to track changes in the permeability of the deposit over time. The results of experimental studies of transport and elution of highly concentrated emulsions from granular structures are also presented. This enabled tracking of changes in flow resistance of the emulsion through the porous bed in time. Moreover, the development of the mathematical model, which allows us to define the relationship between the bed blockage degree and the concentration of the emulsion internal phase could be the result of the experimental works. The results of such studies are very widely used in practice, among other things, in the issues of migration of pollutants, such as petroleum substances, in the soil layers. The development of knowledge in this field may contribute to the optimization of existing oil recovery techniques and methods of remediation of soil from organic substances.

Key words
Emulsion, porous media, multiphase flow

Introduction
Industrial development led to increased consumption of oil products, used as a source of energy or materials for industry. These substances are highly toxic and mutagenic and pose a serious threat for ground and water environments. They can enter the soil and groundwater as a result of various leaks and disasters, and have the ability to penetrate all living organisms inhabiting the affected area, causing irreversible changes. Furthermore, the reduction of crop production can occur due to the presence of oil products in the structure of the soil. Therefore, knowledge about the flow of oil substances through porous media is of great importance, as it can be useful during estimation of the contamination scale and for operations of the removal of such contaminants from the soil. During the spillage of a petroleum substance, taking of appropriate decisions for dealing with the contamination is important. In such cases the most important thing is to properly estimate the risks caused by the spread of the pollution, both in the structure of the soil and in the groundwater. The contamination of these waters can have far-reaching consequences and lead to the poisoning of a much larger ecosystem. Therefore, the correct prediction of the movement speed of contaminants through granular layers and when and at what concentrations they will reach the groundwater is of great importance. Quickly taking the appropriate steps and selecting the best remediation methods will prevent the further spread of contaminations and will also significantly reduce any costs related to the removal of their effects.

When the multiphase fluid flows through the porous medium, the individual phases can mix together, which results in the formation of emulsion systems. Emulsion flow in porous media is different from the independent movement of the individual phases [1], and therefore must be considered separately. The mechanisms, that appear here, need to be taken into account to describe the complex nature of such flows. This can be helpful in understanding and predicting the way in which emulsion systems behave during movement through a porous medium. This knowledge can be useful in obtaining of a comprehensive picture of multiphase flow through

porous media. Although, the issues of the flow of various fluids through porous media can be found in the literature [2, 3, 4], they do not refer to the flow of the emulsions. Knowledge on the emulsion flow through porous media can be used in many practical applications. Understanding the phenomena of the flow of the emulsion is immensely important in developing methods for remediation of soils from the organic liquids, which entered into them as a result of various leaks, failures and accidents [5, 6].

The flow of emulsion through the granular medium depends on the properties of medium and emulsion. Emulsions, as two-phase systems, behave differently than one-phase fluids. Parameters such as emulsion stability, concentration, droplet size and interfacial interactions are important. The concentration of the dispersed phase exerts a strong influence on the rheological properties. O/W emulsions with a concentration less than 50% exhibit Newtonian characteristics, and those with higher concentrations have non-Newtonian ones [1, 7]. When the concentration of emulsion is up to 50%, there is a linear dependence of the pressure drop from the flow rate, which means that Darcy's law can be used for the description of the flow. In the case of concentrations greater than 50% there is no linear relationship of the pressure drop and the flow rate, which suggests non-Newtonian behavior of emulsion. The phenomenon can be explained as the result of the forces of attraction and repulsion present between the droplets. For emulsions with low concentrations, repulsive forces acting between the droplets are sufficiently large compared to the attractive forces, which means that there is minimal aggregation. However, in the case of highly concentrated emulsions, distances between the drops are small and the repulsive forces are reduced, hence the attraction will lead to the formation of aggregates and the coalescence and flocculation will occur [8]. The aggregates rotate as single particles at low shear rates, which results in high fluid viscosity. When the shear increases (the higher flow velocity), the aggregates break up, causing a decrease in the viscosity of the system. This explains the observed non-Newtonian behavior of highly concentrated emulsions [9].

To describe the process of the flow of oil in water emulsions in the porous medium it is important to specify if they can be treated as homogeneous liquids. The assumption that the fluid is a continuous medium can be stated when the emulsion droplets are very small compared to the size of the flow channels. In such cases the influence of microscopic droplets of the emulsion on the flow can be totally ignored [10]. However, in most practical cases, the presence of droplets in the bed cannot be omitted, due to the fact that their sizes are not much smaller than the pore sizes, but even larger than the pores [7]. The reduction of the bed's relative permeability occurs when the O/W emulsion flows through the porous medium. This phenomenon is connected with the size of oil drops. When the droplets of the internal phase are larger than the pores, they can become an effective blocking agent. In actual cases, the oil droplets and pores have a wide range of sizes. Thus, a small amount of emulsified oil may block the flow very effectively [11]. Blocking of the flow channel by emulsion droplets is called the "straining" mechanism [1] and researchers [10, 11] have found that it is mostly caused by permeability reduction. They also observed that in the gaps or pockets the droplets with diameters smaller than the pore size are also captured [12, 13]. It was concluded that the reduction of permeability can also be caused by a different mechanism, called "interception" [1, 9]. The emulsion droplets can be trapped in a porous medium due to the attachment to the pore walls under the action of van der Waals forces and hydrodynamic forces. However, this mechanism has only a small impact on the overall reduction of permeability [14]. In conclusion, there are two capture mechanisms: straining and interception. Straining occurs when the emulsion droplet is trapped in a pore with a smaller size than the drop diameter. Interception is when droplets attach themselves onto the solid surface and pore walls. Capture of emulsion droplets effectively reduces permeability and diverts flow to large pores, through the reduction of pore diameter.

The issues of emulsion flow through porous media can be used to describe methods of remediation of soils contaminated with petroleum substances [15]. In such cases, the techniques used are based on gravitational or pressure elution processes. Gravitational elution often fails to give satisfactory results, so pressure elution is applied to enhance the process. It is based on injecting a lower viscosity fluid into a bed using a pump, which allows the fluid to flow through the bed and wash out the oily substances that residue upon deposit. For both in situ and ex situ cases, the eluting liquid is forced into the contaminated soil. Soil remediation methods based on liquid flow are relatively simple technologically and characterized by high values of coefficient of elution, and thus high efficiency. This is a widely used practice also in the oil extraction industry and it refers to the concept of EOR (Enhanced Oil Recovery). Secondary and tertiary extraction methods are based on the pumping of elution liquid through a bed, which is often a solution of water, salt and various surfactants. The flowing liquid can carry off a significant amount of oily substance trapped in the reservoir, whose production, with the use of other methods, causes many difficulties [16]. There are several scientific works concerning the important

role of emulsions in improvement of microscopic displacement efficiency in chemical EOR methods. Investigations on this essential issue have been exactly and thoroughly described by the researchers [17, 18]. It can be found that the main mechanism of EOR efficiency improvement is the reduction of surface tension of the displacing fluid or reduction of interfacial tension between the displacing and displaced fluid.

Experimental studies on the emulsion flow through the porous bed, which can be found in literature, relate largely to a low concentration of emulsions (up to 20% of the internal phase). There is a lack of experimental data for emulsion systems with inner phase concentrations greater than 50%. The behavior of highly concentrated emulsions in the porous media is different from the transport of low concentrated systems, as they exhibit characteristics of shear thinning fluids. Changes of the flow rate through the bed will also cause a change in viscosity of the examined emulsions, which in turn will affect the flow resistance [19]. This paper presents studies on emulsion flow, with various concentrations, through a granular bed. It allowed us to track changes in the permeability of the deposit over time and to determine changes in the structure of the emulsion flowing out from the reservoir during the process. The results of the experimental studies of transport and elution of highly concentrated emulsions from granular structures are also presented. This enabled tracking of changes in flow resistance of the emulsion through the porous bed over time. Also there is a lack of universal mathematical models that account for the parameters of fluids and deposits, enabling a reliable way to predict the rate of change of the relative permeability and the concentration of the oily substance during flow through the porous medium. Therefore, the development of the mathematical model, which allows the definition of the relationship between the degree of bed blockage and the concentration of emulsion internal phase could be the result of the experimental works. In this paper, studies of the flow of emulsions through granular deposits, at different flow rates of liquids, are presented. The analysis covered emulsions, whose share of the internal phase exceeds 50% and, for comparison, less than 50%.

Experimental apparatus
To perform studies on the flow of emulsions through granular media, the experimental apparatus was designed, whose picture and scheme are presented in Fig. 1 and Fig. 2, respectively. It consisted of the following elements: high-speed stirrer with a stainless steel tank (1), dosing membrane pump (3) with a pulsation damper (4) and horizontal cylindrical measuring column (7) filled with granular material. The test stand has a measuring system included: two flowmeters (5), two temperature sensors (2) and a pressure transducer (6). The system was connected to a computer and with special software, which allowed the continuous monitoring and acquisition of parameters such as the pressure at the inlet to the bed, the temperature of examined fluid and the inflow and the outflow rate of liquid from the bed.

Fig. 1. Picture of research equipment
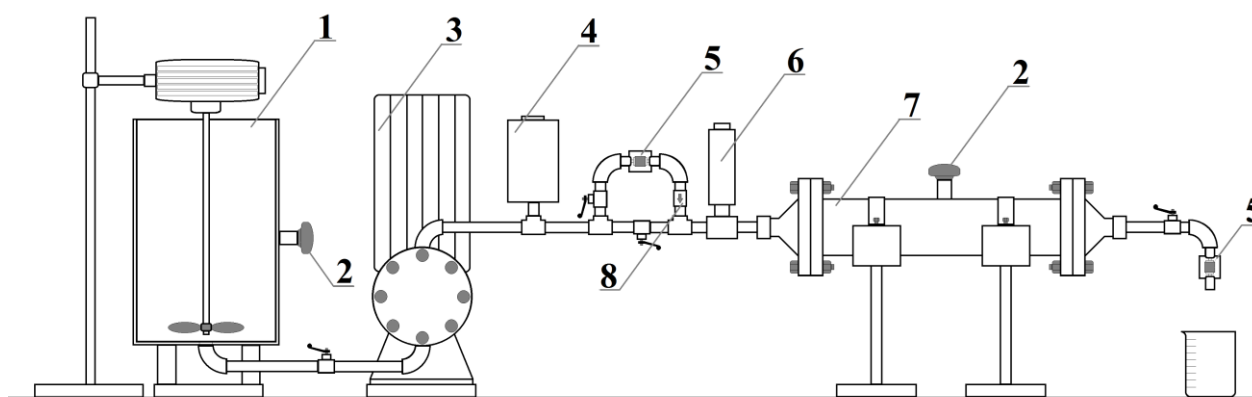*Source: Author's*

Fig. 2. Scheme of research equipment: 1- high-speed stirrer, 2 - temperature sensor, 3 - pump 4 - pulsation dampener, 5 - flowmeter, 6 - pressure sensor, 7 - column with the bed granular 8 – non-return valve
Source: Author's

Experimental media

During the studies, glass microspheres were used as model deposits, with particle size fractions in the range of 200 - 300 µm with a porosity of 0.34, in the range of 100 - 200 µm with a porosity of 0.34, and in the range of 90 - 150 µm with a porosity of 0.33. Alumetal - Technik in Lodz (Poland) was the manufacturer of used glass beads. To examine the flow and elution of emulsions from porous deposits oil-in-water emulsions were prepared as a model fluids, where the continuous phase was tap water (η = 0.001 Pa·s, ρ = 996 kg/m^3 at 22°C) while the inner phase was a vegetable oil (η = 0.06 Pa·s, ρ = 887 kg/m^3 at 22°C). The emulsions systems had different volume concentrations in the inner phase, which equaled 20, 40, 60 and 70% (see Tab. 1). An emulsifier Rokacet 07 (Exol PCC) of 2% volume was used. The precisely measured volumes of emulsion components (water, oil and surfactant) were thoroughly mixed. Emulsification was performed using a high-speed homogenizer (10000 rpm), and the mixing time was 500 s. For the purposes of a single measurement, 2.5 l of emulsion was prepared. To determine the rheological properties and the structure of formed emulsions, a rotational rheometer Rheotec RC20, Nikon microscope Alphaphot 2 YS2 and Turbiscan Lab Expert were used.

Table 1. Emulsion composition

Emulsion concentration [%]	Continuous phase amount [ml]	Inner phase amount [ml]	Emulsifier concentration [%]
20	2000	500	2
40	1500	1000	2
60	1000	1500	2
70	750	1750	2

Source: Author's

Rheological measurements

Based on rheological studies of the emulsions with different volume concentrations of the oil phase, it was possible to present flow curves in the form of a dependence of viscosity on shear rate in Fig.3. It can be seen that the emulsions with lower concentrations (50%) exhibit the properties of Newtonian liquids, and emulsions with greater participation of the internal phase display characteristics of shear thinning fluids.
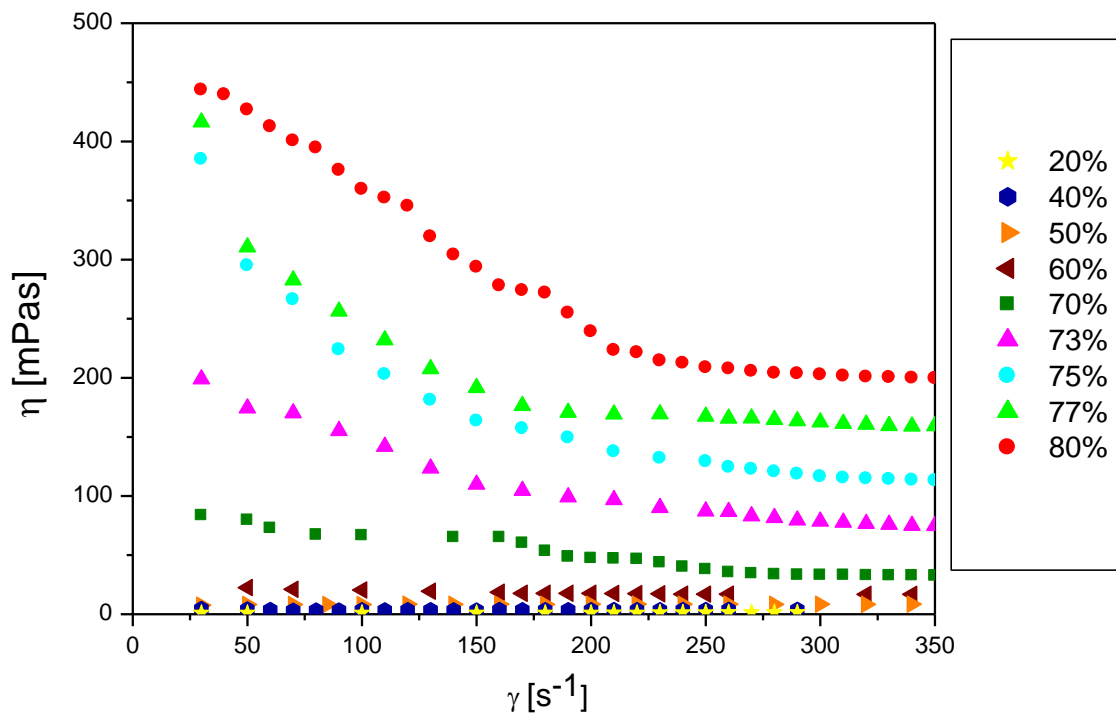
Fig.3. The dependence of viscosity on shear rate for various concentrations of the emulsion oil phase
Source: Author's

Experimental procedure

The research methodology was developed to ensure optimal conditions and the repeatability of tests. At the beginning, a strictly defined amount of glass microspheres was weighed and placed in a measurement column (7). During the tests, only water was pumped at first through the granular bed in the column, until the pressure at the inlet to the bed reached a constant value, i.e. when steady state was obtained. After that, emulsion was pumped through the bed until the steady state was obtained. Then, again the flow of pure water took place. With this methodology, the simultaneous examination of flow and elution processes and observation of the flow resistance changes was possible using a single measurement. By comparing permeability measured for water flow through the reservoir before and after the passing of emulsion through the deposit, it was possible to determine the degree of blockage.

Results and discussion

As a result of the experimental work, it was possible to track changes in flow resistance of the bed during the process. This made it possible to create a graph of the pressure drop dependence Δp at the inlet to the bed from time t. Fig. 4 presents exemplary test results for emulsions of different concentrations, flowing through the bed with a particle size in the range of 90-150 μm. According to the test procedure, clear water flowed first through the bed, followed by a flow of emulsion and water again. The moments, in which successive flows began, were marked with the vertical lines on chart.
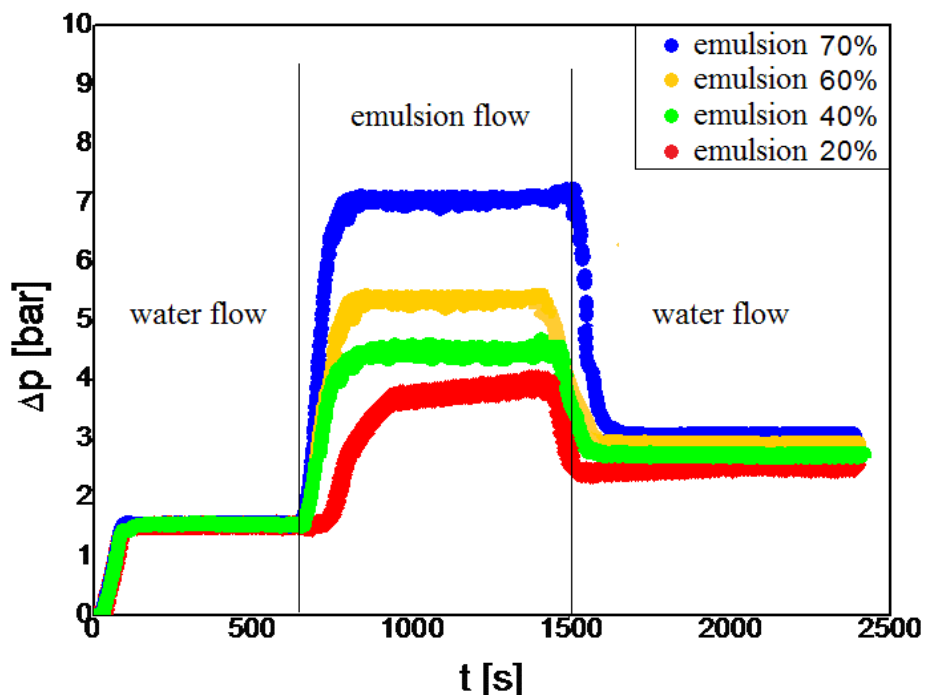
Fig. 4. Dependence of pressure at the inlet to the bed from the time for the emulsion with different internal phase fractions - bed 90 - 150 µm, length 50 cm

Source: Author's

In the first phase of the process, when the water was flowing through the bed, inlet pressure values were repetitive for each flow, which means that the same water permeability was obtained in each case. From the moment when the emulsion began to flow, the inlet pressure started to increase until the steady state was reached. The increase in pressure was due not only to the increase in the viscosity of the flowing liquid, but also to the fact that the oil droplets blocked the flow channels, as was explained in the literature [20]. The phenomenon of stopping of the emulsion inner phase droplets inside the bed structure and the consequent blocking of flow paths is called "straining" and was described in detail in work of Soo and Radke [12]. The increase in inlet pressure was, however, greater with higher concentrations of the emulsion. For a 20% emulsion, a gradual increase in Δp can be observed before the steady state is reached, while for an emulsion with an internal phase of 70% there was a rapid increase in pressure and steady state was achieved faster. This phenomenon can be explained by the fact that for emulsions with a low concentration, the amount of oil droplets is smaller and the time at which all the places in the bed (that can blocked) are filled is longer. In the case of emulsions with higher concentrations, the amount of oil droplets is large, so they quickly settle in the bed paths and block the flow causing the increase in pressure. The pressure value achieved in steady-state during the emulsion flow, at 20% concentration, was about 3.5 bar, while for the emulsion with 70% internal phase was more than 50% grater. This means that flow resistances are not directly proportional to the concentration of the flowing emulsion.

Once the steady state has been reached, the water was pumped again through the bed. There was a sudden drop in pressure and a rapid achievement of a new steady state. However, the new steady state was not reached at the level before the flow of emulsion, but the pressure drop values were higher. This means that a part of the oil phase was trapped in the bed and blocked the flow paths. The pressure drop values during the repeated water flow through the bed were dependent on the concentration of the emulsion, which previously passed through the bed. In the case of processes where an emulsion with a higher concentration was flowing through the bed, the pressure drop values during the washout were higher than those for the lower concentrated emulsions.

During flow and elution of the emulsion from the bed, the outflow rate of liquid from the bed was also measured in time. Exemplary results of these tests, corresponding to the cases discussed above, are shown in Fig. 5. There is a direct relationship between the pressure drop at the inlet and the outflow rate from the bed. This is due to the operation of the apparatus, i.e. the characteristics of the pump, where defined flow resistances cause specific efficiency.
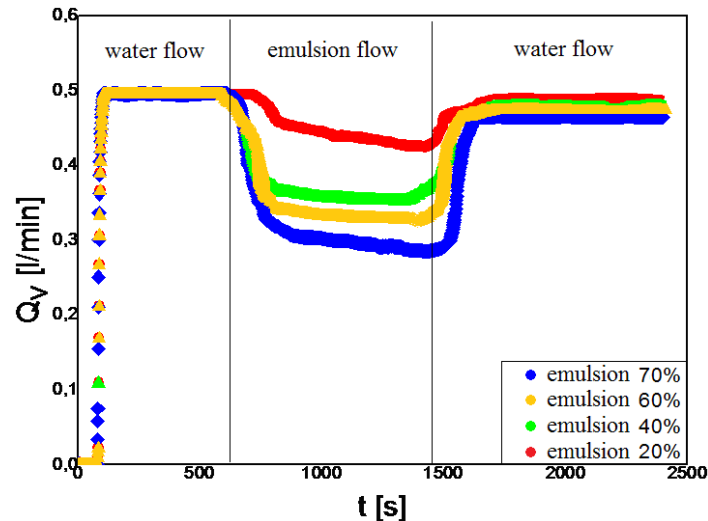
Fig. 5. Dependence of the outflow rate from time for the emulsions of various concentrations - bed 90-150 µm, length 50 cm

Source: Author's

The assessment of bed permeability reduction

This work was further focused on the issue of the pressure drop values at the flow of water through the clean bed are different from values obtained for the bed through which the previous emulsion flowed. Results for the steady states determined before and after the flow of the emulsion through the bed were analyzed. To compare these two states, the relative permeability of the bed and the degree of blockage of the bed were calculated. For this purpose, the classical theory of Darcy was used, whereby bed permeability k can be determined by the following relationship:

$$k = \frac{\eta Q_v L}{A \Delta p} \tag{1}$$

where: k – bed permeability, L – bed length, Δp – pressure drop at inlet to the bed, η – liquid viscosity, A – bed cross section, Q_v - flow rate

For comparative purposes, the concept of relative permeability was introduced. Relative permeability is expressed by the ratio of bed permeability k_p, determined for the flow of water through the clean deposit, permeability k_k, defined for the flow of water through the bed after the flow of the emulsion:

$$k_r = \frac{k_k}{k_p} \tag{2}$$

If the relative permeability determines what fraction of the bed pores is available for the flow (where the flow actually takes place), it can be stated that the bed blockage will determine the pore fraction that is not available for flow. Considering the above relationships, one can write that the degree of blockage of the deposit S_r can be determined according to the formula:

$$S_r = 1 - k_r \tag{3}$$

In Fig. 6 and Fig. 7 the relative permeability dependences from the degree of bed blockage and from the concentration of the emulsion flowing through the bed are shown respectively. The graphs present the results for deposits with grain fractions of 90-150, 100-200 and 200-300 µm. In the case of larger grains, it was possible to carry out experiments for higher concentration emulsions using the test apparatus, so the results also include emulsions with an internal phase content of up to 80%. Above this concentration the phase inversion occurs, so studies were limited to this value. At high concentrations in the range of 80% and greater (Fig. 3), slight changes in the emulsion inner phase content cause a significant increase in the viscosity of the fluids and thus an increase in flow resistance through the bed. This results in changes in the course of the trend

lines describing variations in the permeability and in the bed blockage, as can be observed in Fig. 6 and Fig. 7, respectively.
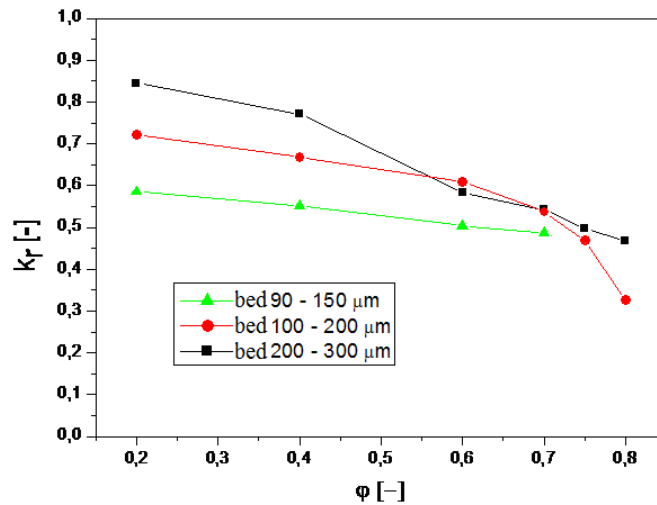

Fig. 6. Changes of relative permeability with emulsion concentration (L – 0.5m, vegetable oil)
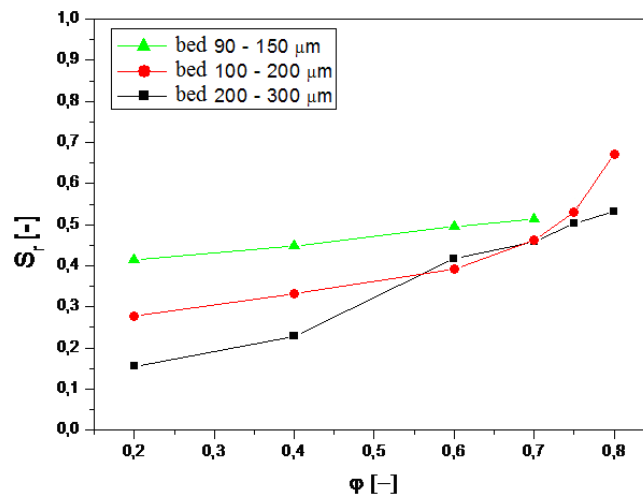*Source: Author's*

Fig. 7. Changes of the bed blockage with the concentration of the emulsion (L - 0.5m, vegetable oil)
Source: Author's

The flow behavior has been discussed through the analyzes of changes in the degree of blockage (see Fig. 7), with respect to the content of internal phase of the emulsion. It can be stated that S_r values increase as the concentration increases for each analyzed bed. For a bed with a particle size within 90-150 μm, it can be seen that for a 20% emulsion the degree of blocking was about 0.42, while for an emulsion with an internal phase of 70% it was up to about 50%, which means that half of the pores were blocked by the oil phase droplets. Considering a bed with larger grains, i.e. a 200-300 μm, for a 20% emulsion only 15% of the flow pathways were blocked, and for 70% emulsion this value reached about 40%. It is also noteworthy that differences in the degree of bed blockage for the analyzed fractions are decreasing as the concentration of the oil phase of the emulsion increases. In the case of highly concentrated emulsions, the difference between the degree of blockage is within a few percentage points, while for the emulsion with lower concentration it is up to 40%. This means that for the emulsions with a high content of internal phase, the size of the bed granules is not as significant for the degree of deposit blockage as for emulsions with a low concentration.

Conclusions
The paper presents the results of experiments relating to the flow and elution of emulsions with different concentrations of internal phase in a porous bed. During the transport of the emulsion, a gradual increase in flow resistance was observed, the intensity of which depended on the proportion of the inner phase of the emulsion. The steady state was achieved fastest for deposits with the highest grain fractions. The value of the

pressure drop achieved in the steady state was also greatest for the highly concentrated emulsions, but it resulted not only from the same emulsion viscosity but also from the effect of blockage of the bed by oil drops.

Using a test procedure involving the pumping of water, emulsion and water again through the bed, it was possible to determine the degree of blockage of the bed by oil droplets. This was done by comparing the bed permeability at the flow of water through a clean bed with permeability at the flow of water through the bed, through which the emulsion previously flowed. Based on this work, it was found that the degree of bed blockage increases with increasing concentration and this dependence has been quantified. It has also been stated that the size of the bed grains has a greater effect on the degree of blockage in the case of low concentrated emulsions.

The results of the research and the presented analysis gives the opportunity to estimate the value of such an important factor as the degree of blockage of the deposit. This will make it possible to predict how the flow of a particular emulsion affects the bed through which it flows. These issues can be very useful in processes of soil cleaning from a variety of organic compounds and for various methods in the course of the recovery of crude oil, wherein the flow of emulsion through the bed is important.

References
[1] F. A. L. Dullien, Porous Media Fluid Transport and Pore Structure, Acad. Press Inc, San Diego, California, 1992

[2] M. Ahmadlouydarab, Z. S. Liub, J. J. Fenga, Relative permeability for two-phase flow through corrugated tubes as model porous media, Int. J. Multi. Flow, 47, (2012), 85–93

[3] E. Idorenyin, E. Shirif, A new simulation model for two-phase flow in porous media, Braz. J. of Pet. and Gas, 6, 1, (2012), 001-018

[4] T.F. Tadros, Emulsion Formation, Stability, and Rheology, Wiley-VCH Verlag GmbH & Co. KGaA, 1–75, 2013

[5] J. Parker, U. Kim, P. Kitanidis, M. Cardiff, X. Liu, G. Beyke, Stochastic cost optimization of DNAPL remediation – Method description and sensitivity study, Environ. Model. Softw., 38, (2012), 74-88

[6] A.N. Piscopo, J.R. Kasprzyk, R.M. Neupauer, An iterative approach to multi-objective engineering design: Optimization of engineered injection and extraction for enhanced groundwater remediation, Environ. Model. Softw., 69, (2015), 253-261

[7] Z. E. Heinemann, Fluid flow in Porous media, Texbook Series, 1, Leoben, 2005

[8] T. F. Tadros, Rheology of Dispersions: Principles and Applications, ISBN-13: 978-3527320035, 2011

[9] J. Török, J. Tóth, G. Gesztesi, Polydispersed O/W emulsions in porous media: Segregation at low-tension conditions, J. Coll. Int. Sci., 295, (2006), 569–577

[10] W.K. Vidrine, C.S. Willson, K.T. Valsaraj, Emulsions in porous media I. Transport and stability of polyaphrons in sand packs, Coll. Surf. A, Physicochem. Eng. Asp., 175, (2000), 277–289

[11] A. Cortis, T. A. Ghezzehei, On the transport of emulsions in porous media, J. of Coll. and Int. Sci., 313, (2007), 1–4

[12] H. Soo, C.J. Radke, The flow mechanism of dilute, stable emulsions in porous media, Ind. Eng. Chem. Fund. 23, (1984), 342–347

[13] S. Cobos, M.S. Carvalho, V. Alvarado, Flow of oil–water emulsions through a constricted capillary, Int. J. Multi. Flow, 35, (2009), 507–515

[14] J. Li, Y. Gu, Coalescence of oil-in-water emulsions in fibrous and granular beds, Sep. Pur. Tech., 42, (2005), 1–13

[15] S. Crawford, J. Clifford, K. David, W. John,. Effects of emulsion viscosity during surfactant enhanced soil flushing in porous media. J. Soil Cont., 64 (1997), 355-370

[16] X. Fu, R. H. Lane, D. D. Mamora, Water-in-Oil emulsions: flow in porous media and EOR potential, SPE Canadian Unconventional Resources Conference, 2012

[17] A. Bera, A. Mandal, T. Kumar, Physicochemical Characterization of Anionic and Cationic Microemulsions: Water Solubilization, Particle Size Distribution, Surface Tension, and Structural Parameters, J. Chem. Eng. Data 59, 8 (2014), 2490-2498

[18] A. Mandal, A. Bera, Modeling of flow of oil-in-water emulsions through porous media, Pet. Sci. 12, 2 (2015), 273-281

[19] J. Cai, C. Li, X. Tang, F. Ayello, S. Richter, S. Nesic, Experimental study of water wetting in oil – water two phase flow—Horizontal flow of model oil, Chem. Eng. Sci., 73, (2012), 334–344

[20] V. A. Tabrizy, Relative Permeability Relationship with Environments of Deposition, Pet. Univ. Techn., Fac. Pet. Eng., Dep. of Pet. Eng., Iran, Ahwaz, 2006

Karolina Nowak, Adrian Smagur
Lodz University of Technology, Faculty of Technical Physics, Information Technology and Applied Mathematics
Wólczańska 215, 90-924 Łódź, karolina.nowak@dokt.p.lodz.pl, adrian.smagur@gmail.com

HAND GESTURES PROVIDED BY LEAP MOTION FOR USER INTERFACE OF INTERACTIVE GALLERY

Abstract
In the digital age, more and more artists are starting to present their works in an interactive way. Due to the rapid progression of the virtual environment and its attractiveness, it appears that new explorations of intuitive and user-friendly galleries are required. We created a draft of a computer application interface and then prepared a special gallery driven by different hand motions performed in mid-air. We conducted research of our proposed solution to compare these gestures and to find out how it is being perceived by people from outside the IT industry.

Key words
interactive gallery, user interface, hand gestures, Leap Motion, Processing

Introduction
Presenting artistic works as an interactive gallery is getting more and more popular since it is more easily accessible to the masses. People can examine all creations anywhere using only their notebooks or smartphones. Many experiments with design and running this type of application were carried out. Normally, all digital images are displayed in a flat 2D image space. The 3D technique allows users to interact and walk through a virtual environment [1]. This idea can be as innovative as the proposition of changing the application controller. Eye, hand and body movement and ideas to measure gestures became popular decades before, but only the last ten years brought major breakthroughs that have since become widely known [2]. However, for the present, there are only a few galleries driven this way. We decided to prepare a special application controlled by hand gestures to increase its accessibility. We wanted to verify the presupposition a computer can sense finger movements, including the computer image zoom, rotate, move, instruction, precise control, and other empty writing, to one hundredth of a millimeter [3].

Related work
Kauri et al. [4] studied various techniques of hand gesture recognition. Firstly, they classified static and dynamic gestures specified as hand postures and gestures. They are similar as they can be recognized by shape, orientation and finger flex angle. The most significant difference is ability to identify motion with its speed and direction. As we planned to design the interactive gallery navigated by hand, we needed to use dynamic gestures.

Authors of that article [4] proposed a classification of hand gesture recognition techniques. There are three methods based on sensors, vision and depth. The first one draws on data from sensors attached to the hand. It can be put on the skin directly or mounted on gloves. The second method uses cameras which capture a series of images. The user does not wear anything as all processes and analyses are conducted on photographs. The last one also embraces cameras, but the main idea was to capture a sense of depth. However, the Kinect device launched by Microsoft uses RGB images where the depth of objects can be found. We decided to work with a vision based technique as it is very natural and intuitive for users. They need to move their hand without any additional sensors and this motion is well-recognized. We chose Leap Motion for our application because it is a very popular and easy to use input device these days.

Pambudi et al. [5] created a desktop based game application with Leap Motion technology. They proved that using Leap Motion as a software developer is not complicated and problematic. They defined the grab gesture by determining the Euclidean distance formula between the node of the index finger and the node of the thumb. If this value is smaller than the one specified, it means that user makes a grab gesture. Put gesture

recognition is based on the same formula, but value must be bigger than the referential one. Authors also studied the influence of light intensity on working of a Leap Motion device. They found out that light with more than 45lx intensity can produce such noises that a calibration process is not able to redub them.

Huang et al. [6] used a Leap Motion device in a music creation application. They proposed a simple method for determining object selection from a hand gesture. Each active element is considered as a single, circle framed object with attributes such as coordinate position and object radius. The pointer (denotive hand position) has its coordinates and radius too. The application checks if these coordinates are within the overlapping range. To this end, it computes the distance between the object and hand marker. If the value is smaller than the sum of the element and the pointer's radiuses, they influence each other. The result is saved as a special variable accepting only Boolean values (true and false).

Sanders et al. [7] prepared a special interface to study the potential of virtual engineering laboratories and tested it with Oculus Rift and a Leap Motion device stuck on goggles. They proposed three sizes of buttons that are supposed to be selected. The side of each square equals 5 cm, 2.5 cm and 1.5 cm sequentially. The biggest one is an equivalent of size of 2-3 fingers held together while the smaller one is the size of a standard keyboard key. Authors also tested two ways to compose these buttons: with and without space left between objects. Research showed that users were the most accurate during selecting the biggest button. Denser configuration of elements also impaired the results.

Materials and methods

A. Project plan

At the beginning, we planned our application interface as it is the most major part of the gallery. If users do not know how to use it, they will not become acquainted with artistic works. The application has a few page content categories: title, some information about the author, a list of creations and the presentation of one of the artist's works. We suspected that navigation by hand may be quite problematic for beginners, so we made bigger buttons. The design is simple and all active elements are well-known to computer users (arrows for the next/previous page and X as exit). Fig. 1 presents sketches with the composition of interface elements, including computed dimensions.

B. Implementation

Our interactive gallery is written in Processing language as it is an open source tool for coding within the context of the visual arts. The interface sketches were our reference. We created a very similar solution (Fig. 1), but we decided to hide the left arrow on the first page until the user sees the entire gallery.

We also added a special hover effects for all active buttons. The next/previous buttons change their color to the opposite one – white arrow becomes black while black background alters into white. The exit button in presentation of one artistic work had to get different effect as changing colors made it to be too similar to the disabled parts in backdrop. Now it is getting darker slowly when user points it. The position of his/her forefinger in application is marked as small red circle.
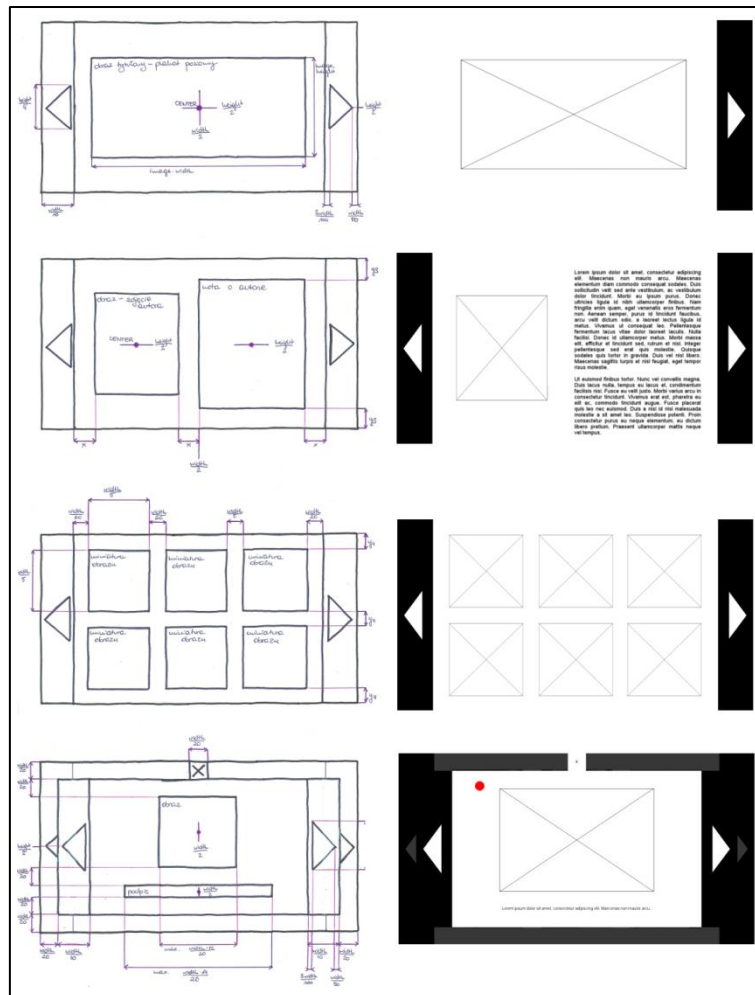
Fig 1. Sketches of gallery interface with dimensions and point (left) and application written in Processing language (right).
Sequentially: application page with title, artist's information, miniatures of works and presentation of creation.
Source: Author's.

There are several functions that had to be implemented:

- Setup function

  It defines the window size and background color of the application. It loads and scales the content of the gallery using additional functions. All images are given by their file paths and are stored in tables with PImage type. The setup function also implements Leap Motion as an individual variable having access to all gesture recognition.

- Draw function

  This function executes in a loop and therefore the view of the application is refreshing all the time. There can be defined gallery pages that are switching with some events' occurring. It has also definitions of all used colors in the application so we can easily test many features.

- Hover function

  It is responsible for checking the position of the pointer and changing the colors of buttons when the forefinger is over them. Since the gallery interface design was planned first, the position of all active elements is known. This function checks which pixels the pointer is on and then decides about buttons' color.

- Click function

  This function executes when the user clicks or makes a circle gesture above an active element. Depending on what kind of item is chosen, the proper action is called.

- Swipe function
  This function detects the appearance of a user's swipe gesture and recognizes its direction. It changes the pages of the application with respect to active gallery view. Depending on the direction of the swipe gesture, the appearing view is chosen (right – previous page or artistic work, left – next one).

C. Controller

A Leap Motion device was chosen to control the application. It recognizes the position and orientation of hands and fingers as it translates them to the bone system. The controller uses optical sensors and infrared light with a 150 degree field of view. There are two IR cameras generating 2D frames of reflected data with speeds up to 200 frames per second. The most effective range of Leap Motion is up to 60 cm above the device. All data analyses are made on the host computer, which gets information through connection with Leap Motion by USB cable. The 3D position of the hand/fingers is calculated on the grounds of 2D frames.

A special library called Leap Motion for Processing is available. It provides hands and fingers recognition with a list of simple gestures. The drawing functions are also included. They can draw not only hands and fingers, but also a whole arm as they use bones and joints. We decided to examine all motions provided by this library: Circle, Screen Tap and Key Tap gestures for the forefinger as clicking on a button and the Swipe gesture for the hand as switching pages of a gallery.

Chan et al. [9] studied one-hand gestures and they found out that tap motion is the most common one. It is identified with selection function as it resembles interaction with remote controllers like mice, touchpad or gaming device. Swipe gesture was second in terms of popularity as respondents used it for directional tasks like moving something or scrolling in any direction. These gestures were frequently used because they are simply and easy to reproduce by everyone, not only people inside the IT industry.
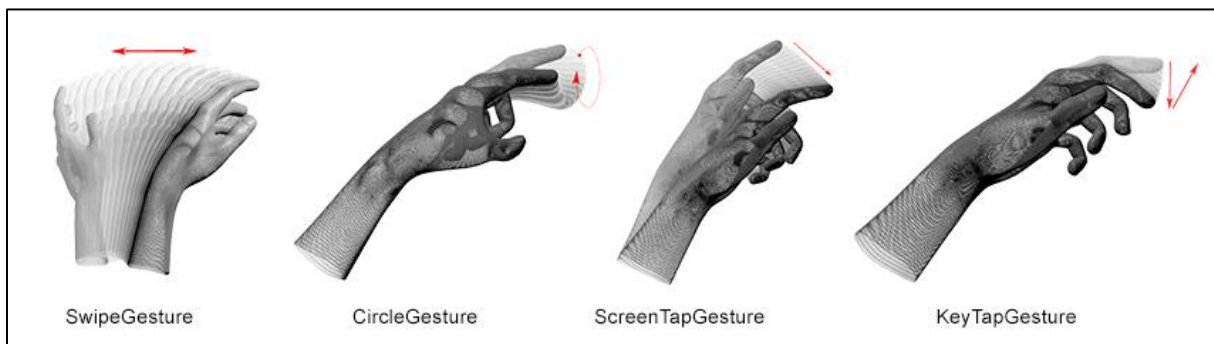

Fig 2. Examined one-hand gestures available in library Leap Motion for Processing.
Source: [10].

Experiment design

We carried out a study of two groups of 10 students (20-22 years old) from Lodz University of Technology from different courses. There were 5 men and 5 women in each group. None of them had used Leap Motion before, but they had a notion of an interactive gallery driven by hand gestures. After the first group test, there were 7 opinions that the gallery sometimes acted peculiarly. Users did not recognize the problem, but we supposed that the application might catch Swipe gesture even if the user did not aim to do it. The second group worked with almost the same version of the gallery, the only difference being that switching pages by hand gesture was turned off.

Respondents were sitting in front of the monitor displaying interactive gallery. They had Leap Motion on table ahead and they could move their hand in mid-air above this device freely. The only constraint was height of the interactive space as it equaled maximum 60 cm.

At the beginning of the study, the whole application was demonstrated. We used a mouse to change pages and select one artistic work from miniatures to zoom in. Then, we presented the instruction of the task: "Please, repeat this navigation, from the first page to the presentation of one work, using only hand gestures". We

switched the mouse for the Leap Motion and started timing. The responders had to go over this task three times since the clicking gesture was changed every time (Circle, Screen Tap and Key Tap).

We made some hypothesis about this research:
- Respondents will have similar time results for Screen Tap and Key Tap because the gestures are conterminous.
- The best time will occur for Circle gesture as it is too specific motion to make it unconsciously.
- Changing pages of interactive gallery by Swipe gesture will be unaffected and convenient for respondents.

Results

In Fig. 3 we present results of our research. There is an average time (with marked measurement error with 95% confidence intervals) that responders needed to complete the task. The red bars concern the first group of students testing the application with Swipe gesture on. The blue ones in the second group working on the gallery with the Swipe gesture are excluded.
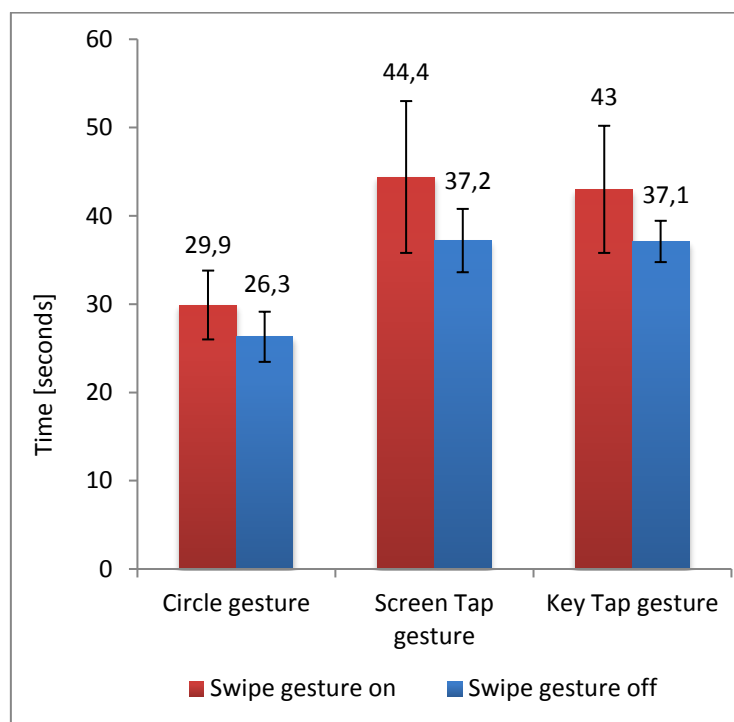
Fig. 3. Chart presenting average time that responders needed to complete the research task.
Source: Author's.

To know more about the results of the research, we calculated some values (Tab. 1). Having variance and variation, we can evaluate how mixed the distribution is. The 95% confidence interval was also calculated and is indicated on the chart (Fig. 3).

We also tested if our results differ significantly from each other (Tab. 2). It is not intuitive as the smaller value is computed, the more meaningful difference is. We calculated Student's T-test which extracts Student's T-distribution widely used in statistics and probability. There are 3 types of this test and we used the one for groups independent on each other as we had two different crops of respondents.

Table 1. Calculated time values for research results. Red values (first for each gesture) attained for application with active Swipe gesture, blue ones (second ones) with Swipe gesture off.

	Circle gesture		Screen Tap gesture		Key Tap gesture	
Average	29.9	26.3	44.4	37.2	43	37.1
Median	30	27	43	36.5	43.5	36
Maximum	40	35	80	51	67	44
Minimum	22	20	31	30	28	32
Variance	43.4	23.1	212.3	36.8	148.4	15.7
Standard Deviation	6.6	4.8	14.6	6.1	12.2	4
Confidence Interval	29.9 ± 3.9	26.3 ± 2.8	44.4 ± 8.6	37.2 ± 3.6	43 ± 7.2	37.1 ± 2.3

Source: Author's.

Table 2. Significant difference between used types of hand gestures. Red values (first for each gesture) attained for application with active Swipe gesture, blue ones (second ones) with Swipe gesture off.

	Circle gesture		Screen Tap gesture		Key Tap gesture	
Circle gesture			0	0	0	0
Screen Tap gesture	0	0			1	0.8
Key Tap gesture	0	0	1	0.8		

Source: Author's.

Discussion

After going over our results, it is obvious that the Circle gesture is working out the best that confirmed our hypothesis. Comparing all averages, minimum and maximum times this motion needs the least to be done successfully. Users learnt this gesture quickly and did it with high precision. There was no problem for them with clicking on one selected element whereas using the Screen Tap or Key Tap gesture was sometimes mistaken by the application. Users moved their hand to get to the designated part of the screen while Leap Motion recognized some gestures. Circle is such a specific motion that the output device did not over interpret it. However, it is so basic that everyone can do it easily.

The interactive gallery with active Swipe gesture was less intuitive for users than the version without this motion. It is evidenced by the times that responders needed to complete the task, as they are significantly different. The minimum time is comparable in both cases, but the maximum time for the gallery with the Swipe gesture is almost the double of the one without this motion. The Leap Motion device recognized this gesture even as respondents did not do it knowingly. This is the reason why our hypothesis was wrong and Swipe gesture did not work well.

Tests with Screen Tap gesture times are the most diverse. Some people completed the task in thirty second but for others it took more than 60 seconds. Because of that range, the confidence interval is the largest for this motion. However, the average time for the Screen Tap and Key Tap gesture does not differ greatly. We can presume that these two motions are very similar for users. Our assumption is evident as the difference between the Screen Type gesture and Key Tap gesture is insignificant (Table 2).

The Screen Tap gesture has the most variable time results. It means that some users did this motion easily while others had troubles with completing the task. It can be caused by a combination of two factors. Firstly, Leap Motion sometimes did not recognize this motion. It is not as specific as the Circle gesture. Users had to learn it from scratch and testing during the experiment took time. Secondly, the Screen Tap is similar to the Key Tap gesture. It was easier for users to make the last gesture because it resembled other moves. If we had changed the order of the gestures, it could have turned out that the Key Tap would have had the most disparate times.

The Circle gesture had the smallest confidence interval because it had the least difference between the minimum and maximum results. This motion is the least differential in terms of time needed for application users to learn and use it successfully. The opposite situation occurs for the Screen Tap gesture.

Conclusions

Our proposal for an interactive gallery driven by hand gestures was tested in terms of four motions. We got the best results for the Circle gesture. This move is very specific so users were not able to do it unknowingly. A circle is not similar to other gestures facilitated by Leap Motion, and so it was recognized by the device effortlessly. What is more, this motion is easy to do so every user could navigate the application without making mistakes.

The Swipe gesture applied as the gallery page changer brought many problems during navigation. Users moved their open hand unconsciously and the Leap Motion device recognized this motion as a Swipe gesture. Pages turned and responders did not know why. This problem is difficult to figure out since users did not do it intentionally. Unfortunately, in our gallery this type of interface element is not a good solution.

Massive elements of interface were helpful in navigation tasks. It was much easier for responders to select one element when it was large. Our assumptions about the low accuracy of hand gesture navigation turned out to be true. Responders with a lack of Leap Motion experience can be the cause for that. We suspect that seasoned users can complete these tasks faster.

In our prospective work, we are planning to add an eye tracking method to our tests. We want to know what responders are looking at and where the marker of a forefinger is at the same time. The results can point to improvements for a more intuitive interactive gallery driven by hand gestures.

References

[1] C. Sinthanayothin, N. Wogwean, W. Bholsithi. Interactive Virtual 3D Gallery Using Motion Detection of Mobile Device. International Conference on Mobile IT Convergence. 2011.

[2] Gergely Sziládi, Tibor Ujbányi, József Katona. Cost-effective Hand Gesture Computer Control Interface. IEEE International Conference on Cognitive Infocommunications. 2016.

[3] He Ling, Li Rui. VR Glasses and Leap Motion Trends in Education. The 11th International Conference on Computer Science & Education. 2016.

[4] Harpreet Kauri, Jyoti Rani. A Review: Study of Various Techniques of Hand Gesture Recognition. IEEE International Conference on Power Electronics. Intelligent Control and Energy Systems. 2016.

[5] Rizal Asrul Pambudi, Nana Ramadijanti, Achmad Basuki. Psychomotor Game Learning Using Skeletal Tracking Method with Leap Motion Technology. International Electronics Symposium. 2016.

[6] Ting-Hsiang Huang, Zhen-Qi Zhuang, Chia-Yen Chen, Bao Rong Chang, Po-Chuan Lin, Yang-Yen Ou. An Interactive Musical Application with Hand Motion and Gesture Controlled Interface. International Conference on Orange Technologies. 2015.

[7] Brian Sanders, Dennis Vincenzi, Yuzhong Shen. Scale and Spatial Resolution Guidelines for the Design of Virtual Engineering Laboratories. W: Jussi Ilari Kantola, Tibor Barath, Salman Nazir, Terence Andre (Eds.). Advances in Human Factors, Business Management, Training and Education. Proceedings of the AHFE 2016 International Conference on Human Factors, Business Management and Society, July 27–31, 2016, Walt Disney World, Florida, USA. 2017. ss. 372-382.

[8] Alberto Scicali, Hans-Peter Bischof. Usability Study of Leap Motion Controller. Conference Proceedings, Conference on Modeling, Simulations and Visualization Methods. Volume 19. 2015. ss. 105-109.

[9] Edwin Chan, Teddy Seyed, Wolfgang Stuerzlinger, Xing-Dong Yang, Frank Maurer. User Elicitation on Single-hand Microgestures. 2016.

[10] Library Leap Motion for Processing. https://github.com/nok/leap-motion-processing/blob/master/reference/leap_gestures.jpg. online: July 2017.

[11] Ionut-Alexandru Zaiti, Stefan-Gheorghe Pentiuc, Radu-Daniel Vatavu. On free-hand TV control: experimental results on user-elicited gestures with Leap Motion. 2015.

Monika Janas, Alicja Zawadzka
Faculty of Process and Environmental Engineering, Lodz University of Technology,
90-924 Lodz, Wolczanska 213, monika.janas@dokt.p.lodz.pl

BIOFILTRATION AS AN EFFECTIVE METHOD FOR REDUCTION OF POLLUTANT EMISSIONS

Abstract
The development of industry and municipal infrastructure is a cause of increased emissions of malodorous substances into the atmosphere. These substances have a negative impact on human health and the environment. To protect the natural environment and human health, innovative methods of reducing emissions to the atmosphere are sought. These methods should be part of sustainable development principles. The work was carried out to assess the effectiveness of biofiltration in the reduction of odorous gas concentrations based on the measurements of biofilter efficiency in a sewage treatment plant. A mathematical simulation of the pollutant emission range in the environment was made to verify its change resulting from the use of a biofilter.

Key words
biofiltration, biofilter, malodorous gases

Introduction
Increased emissions of malodorous substances into the atmosphere are primarily related to industry, agriculture and municipal management. The main cause of their odor nuisance is the presence of odorous organic compounds (aliphatic, aromatic, aldehydes, ketones), as well as hydrogen sulfide, ammonia, sulfur oxides and nitrogen oxides in the emitted gases [1-3]. The malodorous substances coming from these sources have a negative impact on human health. Prolonged exposure to odors may cause depression, fatigue, respiratory problems, headaches, nausea, and eye and throat irritation [4]. Odors, especially volatile organic compounds (reactive organic gases), which are involved in photochemical reactions, are also characterized by relatively high toxicity and environmental harmfulness [5]. Hence, emission reduction and neutralization of malodorous gases is a strategic action from the environmental point of view. Choice of an appropriate technique depends on many factors such as the type of emission source or properties of the emitted gases and impurities they contain [4].

One of the most dynamically developing methods for deodorization of malodorous gases is biofiltration. The essence of biofiltration is the aerobic degradation of pollutants by microorganisms present in the filtering material, which results in the formation of non-toxic compounds that are not harmful to the environment [5-7]. Biological processes are carried out in bio-scrubbers, biofilters and with the use of sprinkling biological beds (three-phase bioreactors). Due to the relatively low investment and operating costs, wide application range and minimal waste generation, biofilters are used mainly in the treatment of malodorous gases [6-7].

The article defines the process of biofiltration as an effective method for deodorization of odorous gases. Attention has been paid to the parameters that must be satisfied by these gases to be treated. The structure of a model biofilter is shown. Taking as an example the Sewage Treatment Plant in Konin, an assessment of the effectiveness of biofiltration in the reduction of odor nuisance was conducted. The assessment was based on the concentration of malodorous substances before and after the installation for biological air purification (biofilter) and a mathematical simulation was performed to test the effects of minimizing the range of airborne emissions.

Biofiltration
Biofiltration is one of the methods to reduce the amount of malodorous gases. It involves passing of contaminated air through a layer of porous material containing microorganisms, where pollutants are removed due to biodegradation [2, 8-10]. During gas flow through the filtering material layer, the pollutants diffuse from the gas phase into the active biolayer surrounding the filtering material particles. In the liquid

phase containing microorganisms and dissolved pollutants, they are decomposed into carbon dioxide, water and biomass. Biological gas purification is based primarily on two processes – the absorption of pollutants in water and their biological decomposition [5, 11-12].

The smooth running of the biofiltration process and high efficiency of gas purification require strictly specified environmental conditions in which the process is carried out. Currently, with regard to construction and applied filling, various types of biofilters are used [13]. Their main component is a layer of filtering material to which gases are fed from the bottom of the perforated pipe system. In turn, the bed is humidified counter-currently and nutrients for microorganisms are introduced with water [12]. To achieve the maximum rate of biodegradation of pollutants, the filter material should provide the most favorable conditions for the development of microorganisms which are the purifying agent. It should be characterized by high porosity and large specific surface area. From an economic point of view, it should have low flow resistance (200-2000 Pa) [13]. In fact, materials of natural origin are good biofilters, particularly peat, compost, bark, wood chips, straw and moss. The efficiency of biofiltration is also affected by physicochemical conditions in the bed which directly determine the state and number of microorganisms. It is crucial to provide an environment that is optimal for their development, including the appropriate temperature, hydrogen ion concentration, redox potential, water content in the environment and nutrient availability [14].

It should also be noted that gases subjected to biofiltration must satisfy certain criteria, the main one being their susceptibility to biodegradation and water solubility. In addition, due to high toxicity to microorganisms contained in the bed, these gases should not contain heavy metals [15].
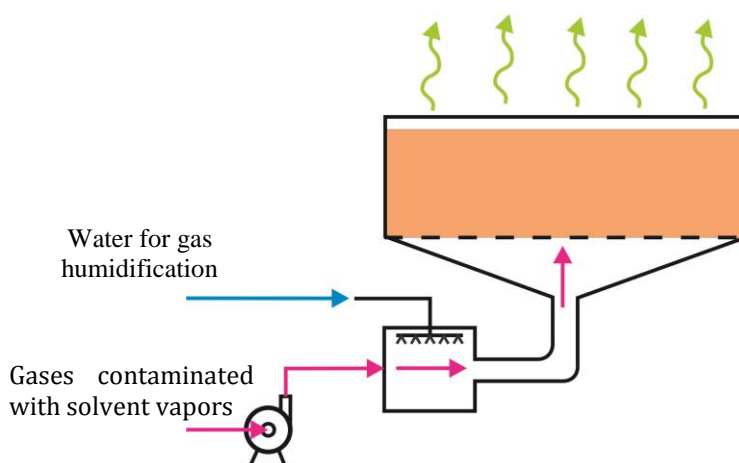

Fig. 1. Technological diagram of the analyzed biofilter
Source: Author's

The object of study
The object of the study was a biofilter used to purify air from the Sewage Treatment Plant in Konin. It is equipped with a biomass tank, i.e. a bioreactor with dispersed biomass, and a compatible machinery consisting of a fan and air humidifier. The whole is connected by ventilation ducts to transport air between the individual elements. This set is integrated with an electrical switchgear consisting of controllers, regulators and relays. The biofilter is connected to the instruments and indicators that control its work to coordinate the system operation. The biomass tank is made of glass-polystyrene laminated material resistant to atmospheric agents and polluted-air condensate. The structure is additionally strengthened with a steel frame made of closed profiles, which is permanently laminated into the tank walls. Radial fans made of stainless steel (A4, grade 316 in accordance with AISI) equipped with vibration compensators are used for air pumping. The whole apparatus is placed in a soundproof case which guarantees that noise levels do not exceed 80dB at 1 m distance.

Technical parameters of the analyzed biofilter:
- the amount of purified air – 6700 m3/h
- bed surface – ca.64 m2
- total amount of biomass – ca.96 m3

- type of biomass – pine bark
- fan motor power – up to 11 kW
- power of humidifier heater – up to 3 kW
- power of other devices – up to 4 kW
- water consumption – up to 140 dm3/h
- biofilter dimensions – 1.7 m × 2.0 m × 5.0 m (Height × Width × Length)

Research methodology
In order to assess the effectiveness of odorous gas emission reduction, the concentrations of individual pollutants were measured. Gas samples were collected three times at weekly intervals, respectively from the discharge end of the fan, from the humidifier where air is supplied from the treatment facilities and from the outlet pipe through which the purified air is emitted into the atmosphere. The samples were collected in accordance with the method described in standard PN-Z-04008-4: 1999P "Air purity protection – Collection of exhaust gas samples (emission) with air-like characteristics and their preparation for analysis by gas chromatography" during dry weather. The tests were conducted in June 2015.

The tested compounds (H_2S, mercaptans, diethylamine, trimethylamine) were determined by sampling the air with the use of a Sensidyne low-flow suction pump equipped with a flow meter and control valve. The assay was performed by gas chromatography with a mass detector after desorption from activated carbon. In turn, the concentration of ammonia, formaldehyde and SO_2 was determined using the LANCOM SERIES II meter from LAND INSTRUMENTS (UK).

A mathematical simulation was performed using the Opa03 program to verify the range of pollutant emissions. This system provides modeling of the range of air pollution from point, line and surface sources using a calculation algorithm compliant with the Regulation of the Minister of Environment no. 796 Dz.U. 87/2002 [16], no. 12 Dz.U. 1/2003 [17] and no. 2181 Dz.U. 260/2005 [18]. The basis for calculations is the Gaussian model of "streaks of pollution" formed by wind and diffusion processes.

Result and discussion
Concentrations of the analyzed pollutants at the inlet and outlet of the biofilter and effectiveness of biofiltration of these compounds are summarized in Table 1. It should be noted that the effectiveness of biofiltration is a function of biodegradability, concentration of pollutants and gas flow, as well as design parameters, including biofilter size and temperature.

Table 1. Concentrations of gases from the biofilter and effectiveness of their reduction

Compound	Concentration		Biofiltration efficiency	Measurement error
	µg/m3			
	Biofilter inlet	Biofilter outlet	%	%
SO2	158	15	91	15
H2S	154	9	94	13
Mercaptans	192	8	96	16
Diethylamine	1 526	133	91	13
Trimethylamine	788	68	91	13
NH3	1 799	163	91	15
Formaldehyde	1 987	188	91	11

Source: Author's

Based on the results presented above, the highest reduction of concentration was observed for mercaptans (96%) and hydrogen sulfide (94%). For other tested pollutants, the effectiveness of biofiltration is 90-91%. However, according to numerous studies, even such high efficiency of the process does not completely eliminate unpleasant odors. Odor nuisance was particularly noticeable directly in the vicinity of communal utilities.

Hong and Park [19] examined the effectiveness of biofiltration to remove ammonia generated during the composting of food waste from the food industry. They used biofilters with two different fillings, working in the same conditions. The research showed nearly 100% neutralization of ammonia generated during the composting process.

Similar results were achieved by Pagans et al. [20] who similarly studied the effectiveness of biofiltration with respect to ammonia produced during the composting of animal by-products. Research showed that in the early days of the experiment, the ammonia removal rate was very high (over 90%), and by the end of the experiment it had dropped significantly (down to 30%).

Biofilters are limited in their ability to remove volatile organic compounds (VOCs), due to the time required for their decomposition, effectiveness of the decomposition and process control. Most VOCs are not readily degraded by microorganisms in the filters and require a longer residence time, which in turn involves the need for larger systems with greater surface area. The effectiveness ranges between 40 and 70% [21]. Table 2 presents effectiveness of the removal of selected odors with the use of biofilters.

Table 2. Effectiveness of the removal of selected odorous substances by biofiltration

Pollutant	Removal effectiveness, %	Concentration, μg/m3
Hydrogen sulfide	99.99	30-3690000
Ammonia	96.4-98.3	1400-580000
VOCs, i.e. volatile organic compounds (converted to butanol)	40-70	140-40000
Aldehydes	75	-
Alcohols	90	-
Aromatic hydrocarbons	40-80	-
Odors	95-99	-

Source: [22]

Lebrero et al. [21] attempted to apply biofiltration using an activated sludge diffusion system (AS). The emitted malodorous substances got directly into the aeration tank where, together with oxygen, they diffused through the sludge to be degraded by appropriate microorganisms. Sludge from the sewage treatment plant containing aerobic bacteria was used as an inoculum. As a result, the reduction of hydrogen sulfide and butanone concentrations was 98-99.5%. Below is a graphical interpretation of the spread of pollutants without and with the use of a biofilter, respectively.
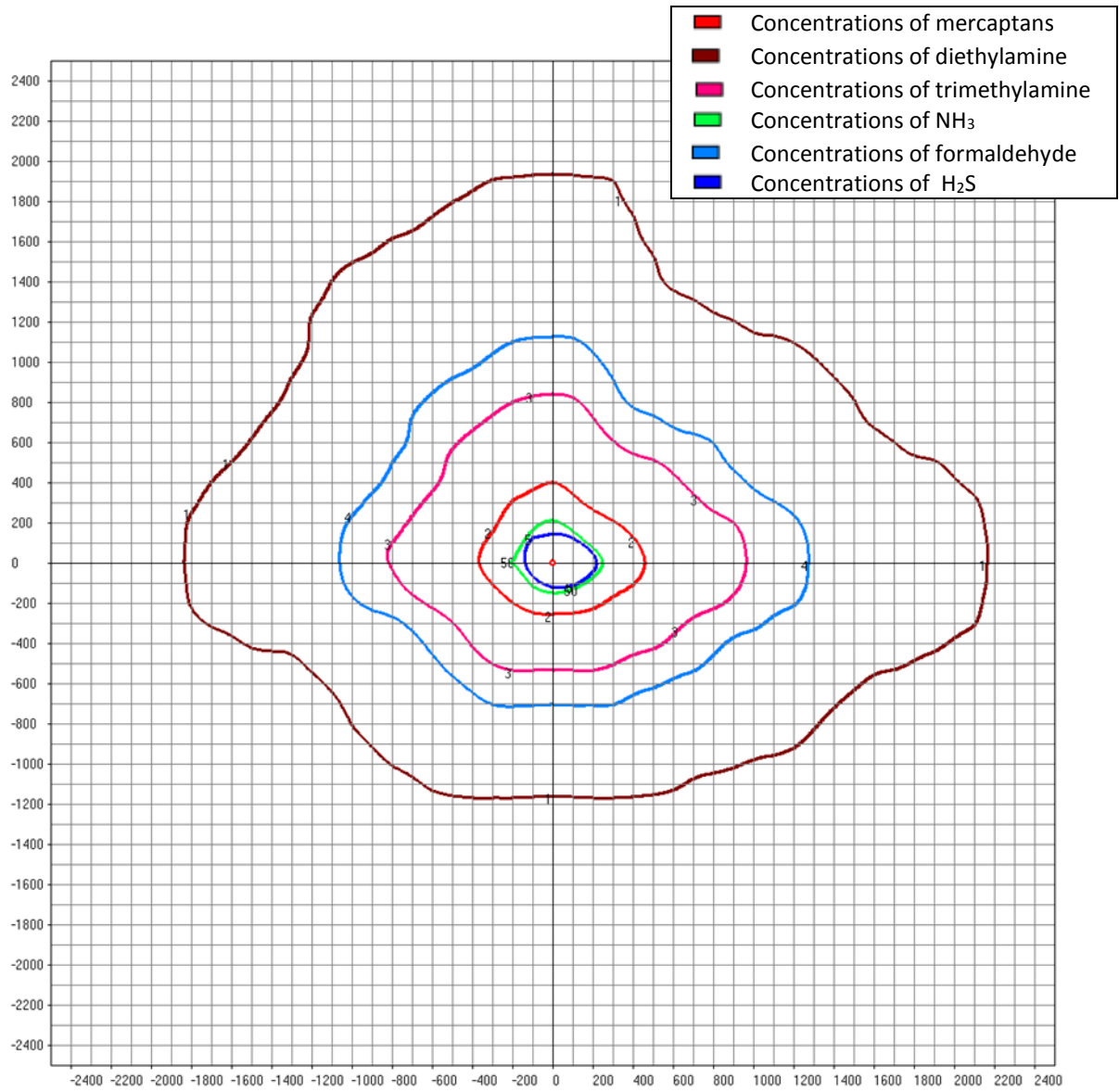
Fig. 2 Graphical interpretation of the spread of pollutants without a biofilter in relation to mean annual values
(distance from the emitter given in meters)
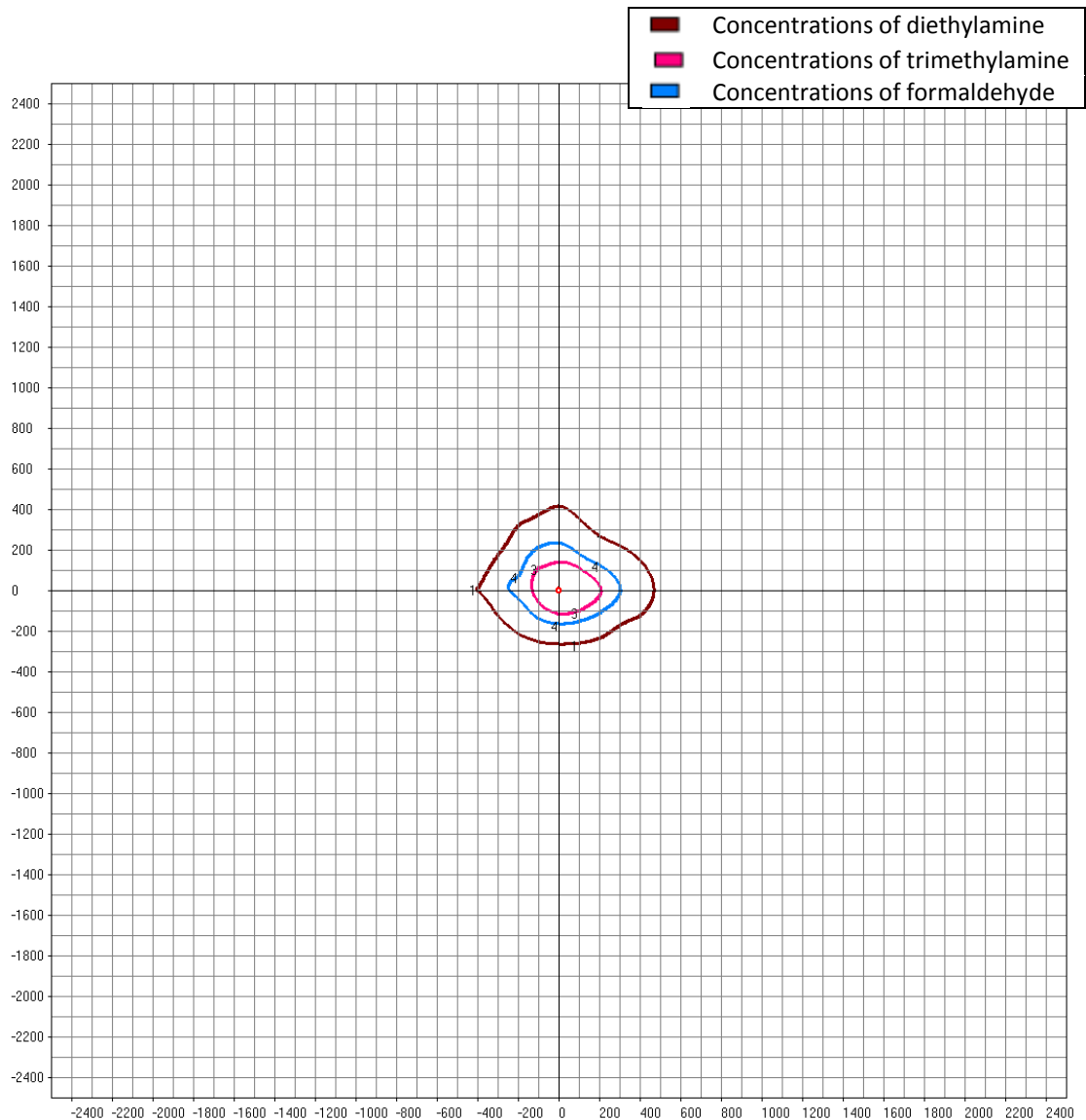*Source: Author's*

Fig. 3. Graphical interpretation of the spread of pollutants with a biofilter in relation to mean annual values
(distance from the emitter given in meters)
Source: Author's

The spread of pollutants is determined primarily by meteorological conditions, topographic features and buildings situated near the source of emission. It should be borne in mind, however, that due to the strong wind currents, the pollutants reach their maximum concentrations sometimes up to several kilometers from the emission source. The performed simulation calculations can be very helpful in air monitoring, as for different atmospheric conditions and terrain roughness they allow us to predict the range of emissions and pollutant concentration on a given surface depending on the source parameters and the amount of pollutants produced.

Summary

The operation of municipal facilities is associated with emissions of harmful chemicals and nuisance odors. The sources of these increased emissions are particularly wastewater treatment plants, where there is direct movement (mixing) or flow of sewage and sludge, as well as large plants where composting or co-composting of waste from food industry is carried out.

Odorous substances include hydrogen sulphide (H2S), ammonia (NH3) and vapors of organic substances i.e. aldehydes, organic acids and ketones, which are a result of microbiological processes. An effective method to eliminate nuisance odors is to limit their emissions by closing (encapsulating) the objects in which these substances are formed and then deodorizing the contaminated air or waste gas streams before they are discharged into the atmosphere.

Deodorization is one of the more difficult issues of the waste gas treatment technology. A low odor detection threshold (the concentration of odorant in the air at which there is a 50% chance of sensing the difference between the smell of contaminated and pure air) of many gases with nuisance odor causes that in most cases it is necessary to remove almost completely the odorous compound [11].

Deodorization of contaminated air can be carried out using a variety of technologies, including absorption, adsorption, condensation and biological methods. However, biological methods, especially biofiltration, are becoming increasingly popular. This method compared to conventional physicochemical methods is characterized by significantly lower investment and operating costs, the possibility of using different filter materials, depending on the type of pollution and the possibility of re-using the applied filter material.
Depending on substances contained in the gas, the efficiency of its purification ranges from 90 to 94% which confirms high effectiveness of this method. Waste gas purification by biofiltration is successfully used in many sectors of the economy and produces satisfactory results [13].

References
[1] R. Lebrero, M.G.L. Rangel, R. Munoz, Characterization and biofiltration of a real odorous emission from wastewater treatment plants sludge, J. Environ. Manage., vol. 116 (2013) 50-57

[2] C. Easter, C. Quigley, P. Burrowes, J. Witherspoon, D. Apgar, Odor and air emissions control using biotechnology for both collection and wastewater treatment systems, Chem. Eng. J., vol. 113 (2005) 93-104

[3] Q. Liu, M. Li, R. Chen, Z. Li, G. Qian, T. An, J. Fu, Biofiltration treatment of odors from municipal solid waste treatment plants, Waste Manage., vol. 29 (2009) 2051-2058

[4] A. Talaiekhozani, M. Bagheri, A. Golic, M.R.T. Khoozani, An overview of principles of odor production, emission, and control methods in wastewater collection and treatment system, J. Environ. Manage., vol. 170 (2016) 186-206

[5] D. McNevin, J. Barford, Biofiltration as an odour abatement strategy, Biochem. Eng. J., vol. 5 (2000) 231-242

[6] S.M. Zarook, A.A. Shaikh, Analysis and comparison of biofilter models, Chem. Eng. J., vol. 65 (1997) 55-61

[7] P. Lewkowska, B. Cieślik, T. Dymerski, P. Konieczka, J. Namieśnik, Characteristics of odors emitted from municipal wastewater treatment plant and methods for their identification and deodorization techniques, Environ. Res., vol. 151 (2016) 573-586

[8] M. Brattoli, G.D. Gennaro, V.D. Pinto, A.D. Loiotile, S. Lovascio, M. Penza, Odour detection methods: Olfactometry and chemical sensors, Sensors, vol. 11 (2011) 5290-5322

[9] M. Latos, P. Karageorgos, N. Kalogerakis, M. Lazaridis, Dispersion of odorous gaseous compounds emitted from wastewater treatment plants, Water Air Soil Poll., vol. 215 (2011) 667-677

[10] E. Pagans, X. Font, A. Sanchez, Emission of volatile organic compounds from composting of different solid waste: Abatement by biofiltration, J. Hazard. Mater., vol. 131 (2006) 179-186

[11] S. Rappert, R. Muller, Odor compounds in waste gas emissions from agricultural operations and food industries, Waste Manage., vol. 25 (2005) 887-907

[12] M. Schlegelmich, J. Streese, R. Stegmann, Odour management and treatment technologies: An overview, Waste Manage., vol.25 (2005) 928-939

[13] B. Mills, Review of methods of odour control, Filtr. Separat., vol. 32 (1995) 147-152

[14] C. Yang, H. Chen, G. Zeng, G. Yu, S. Luo, Biomass accumulation and control strategies in gas biofiltration, Biotechnol. Adv., vol. 28 (2010) 531-540

[15] J.S. Devinny, J. Ramesh, A phenomenological review of biofilter models, Chem. Eng. J., vol. 113 (2005) 187-196

[16] Rozporządzenie Ministra Środowiska z dnia 3 marca 2008 r. w sprawie dopuszczalnych poziomów niektórych substancji w powietrzu (Dz. U. 2008 nr 47 poz. 281)

[17] Rozporządzenie Ministra Środowiska z dnia 26 stycznia 2010 r. w sprawie wartości odniesienia dla niektórych substancji w powietrzu (Dz. U. 2010 nr 16 poz. 87)

[18] Rozporządzenie Ministra Środowiska z dnia 4 listopada 2014 r. w sprawie standardów emisyjnych dla niektórych rodzajów instalacji, źródeł spalania paliw oraz urządzeń spalania lub współspalania odpadów (Dz. U. 201 poz. 1546)

[19] J.H. Hong, K.J. Park, Compost biofiltration of ammonia gas from bin composting, Bioresource Technol., vol. 9 (2005) 12-16

[20] E. Pagans, X. Font, A. Sanchez, Biofiltration for ammonia removal from composting exhaust gases, Chem. Eng. J., vol. 113 (2005) 105-110

[21] R. Lebrero, E. Rodriguez, P.A. Garcia-Encina, R. Munoz, A comparative assessment of biofiltration and activated sludge diffusion for odour abatement, J. Hazard. Mater., vol. 190 (2011) 622-630

[22] I. Sówka, U. Miller, P. Sobczyński, Emisja odorów z procesów kompostowania odpadów komunalnych, Przemysł Chemiczny, vol. 93, issue 15 (2014) 1000-1003

Robert Cichowicz, Artur Wacław Stelęgowski
Lodz University of Technology, Department of Environmental Engineering and Building Construction Installations, Faculty of Architecture, Civil and Environmental Engineering
al. Politechniki 6, 90-924 Lodz, Poland, robert.cichowicz@p.lodz.pl, arturstelegowski@gmail.com

NUMERICAL ANALYSIS OF THE SELECTED AIR PARAMETERS IN THE INDUSTRIAL BOILER PLANT

Abstract
In every boiler plant, including industrial boiler plants of thermal capacity above 2 MW, substantial heat gains are generated during the work of combustion units. As a result, the indoor air temperature raises in the room, which affects thermal comfort of workers operating such technological installations. Therefore, heat removal requires an effective mechanical ventilation system. A numerical analysis of the selected air parameters in a room equipped with combustion devices was undertaken using computational fluid dynamic (CFD) simulations in the DesignBuilder software. This was done for a combustion plant in the "Installation of Thermal Treatment of Sewage Sludge" building, located in the "Group Sewage Treatment Plant" complex of Lodz, Poland. The numerical analysis was based on experimental measurements and the results concerning the personnel work area were compared to the guidelines of the ISO international standard 7730:2005.
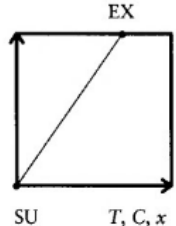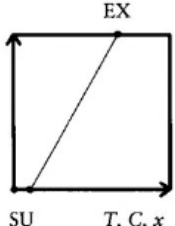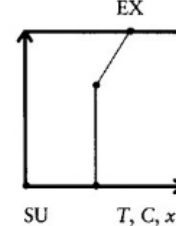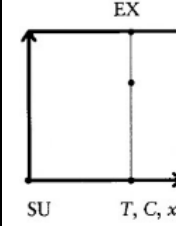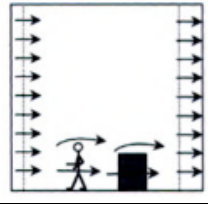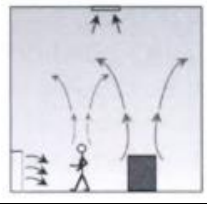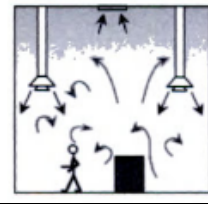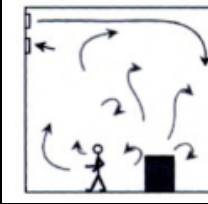
Key words
thermal comfort; air parameters; CFD analysis

Introduction
The operation of combustion devices causes the emission of contaminants such as solid particles, gases, steam and heat [1-2]. The basic issue for industrial ventilation is the removal or decrease of contaminant concentration resulting from industrial processes [1, 4] to provide proper working conditions for the staff operating the industrial plant. Mechanical ventilation can also remove sensible heat gains derived from devices to ensure appropriate air parameters (such as temperature and velocity) in the staff work area [5]. The operation of such installation is based on a system equipped with air supply and air exhaust elements, which are used in general zoning and local ventilation [6, 7].

Additionally, there is a need to correctly calculate the ventilation airflow, which should result from the knowledge of technological processes used in the combustion plant [1, 5, 8]. Table 1 shows the airflow distribution approaches classified into four main ventilation system strategies: piston, stratification, zoning and mixing [9]. For example, the stratification strategy is intended to remove heat gains and air contaminants by supporting the convection and discharge of warmer, polluted air through the supply of low-momentum colder outdoor air. And the mixing strategy assumes providing a uniform distribution of heat and contaminants throughout the ventilated space.

Table 1. Ideal room air conditioning strategies

Strategy				
Description	Piston	Stratification	Zoning	Mixing
Heat, humidity and contaminant distribution*	EX / SU / T, C, x	EX / SU / T, C, x	EX / SU / T, C, x	EX / SU / T, C, x
Application example in a room				
* SU – supply, EX – exhaust, x-axis: T – temperature, C – concentration of contaminants, x – humidity, y-axis: room height				

Source: [9]

The evaluation of regularity of technical and technological solutions for decreasing/removing the contaminant concentration, connected with the operation of combustion units, is possible using the analysis of air parameters in the work area of staff handling such devices. These parameters include air temperature and velocity, as well as humidity, impact of surfaces radiant temperature and the asymmetry of temperature distribution in the room, and are significant environmental factors affecting a sense of thermal comfort [10].

However, air parameters (temperature, humidity and velocity) must be connected with individual factors [10], such as the type of work [11], clothing [12-13] and physiological adaptation to working in hot environments (acclimatization) [14]. Indoor microclimate can be assessed through users' thermal sensation and therefore the PMV (Predicted Mean Vote), as well as PPD (Predicted Percentage of Dissatisfied) ranges, specified in the ISO international standard 7730:2005 [11] can be the indicators of local comfort in industrial buildings.

A calculated value of PMV is compared with 7-step scale of thermal sensation ranging from -3 (cold) do +3 (hot). The PPD index is a function of PMV value, and allows for the estimation of the percentage of population negatively evaluating the thermal environment. Using these indicators is restricted to some conditions such as when ambient temperature does not exceed + 30°C, when mean radiant temperature in the range of + 10 °C to + 40 °C, and when air velocity lower than 1.0 m/s. What is more, its usage can be flawed depending on ethnic and geographical differences [11, 15 - 16].

To assess the predicted thermal sensation in conditions of high air velocity in the room (e.g. with industrial ventilation system), one can use the corrected effective temperature index (CET), which specifies the thermal comfort sensation depending on air temperature, velocity and humidity [17]. The corrected effective temperature can be read from Yaglou graph [18], basing on the indication of dry bulb and wet bulb temperature, and air velocity at a specific point. Another approach to determine the required air parameters in the work area is the Wet Bulb Globe Temperature index (WGBT), defined in the ISO international standard 7243:1989 [14], which specifies threshold limit values for thermal load influencing humans during an eight hour working time in a hot environment. The criteria of thermal load differ depending on solar radiation, metabolic rate (from resting to very hard work) and acclimatization.

Thermal comfort conditions can be assessed using experimental measurements of air parameters at specific points of a room as well as conducting a theoretical analysis of the distribution of air temperature and velocity. Since it can be computationally onerous to analyze air parameters in the stage of designing or verification of technical solutions, the use of computer-aided numerical methods is appropriate [19 - 22].

One of these methods is known as CFD (Computational Fluid Dynamics) analysis and is used in both open-source and commercial software, such as OpenFOAM [23], ANSYS Fluent [24], PyroSim [25], and DesignBuilder [26]. This kind of software can provide a simulation of distribution of air velocity and temperature [27 - 28], as well as aid in optimizing technical solutions [29-30]. The result of CFD analysis, after being compared with experimental measurements, can be useful for assessing the effectiveness of removal or decreasing the concentration of contaminants in the air [31], and evaluating the extent the conditions of thermal comfort at a specific point in a room [27]. However, there is a lack of design criteria of thermal comfort for industrial rooms. Department stores are the closest to the metabolic rate of workers of a boiler plant as they conduct light industrial activity [11, 14]. Therefore, table 2 shows recommended values of indoor air temperature and velocity for light activity of workers in department stores, adopted from the standard ISO 7730:2005 [11].

Table 2. Design criteria for light activity

Comfort category	Metabolic rate	Temperature (summer)	Maximum air velocity (summer)
A		+ 23.0 ± 1.0 °C	0.16 m/s
B	93 W/m2	+ 23.0 ± 2.0 °C	0.20 m/s
C		+ 23.0 ± 3.0 °C	0.23 m/s

Source: [11]

The analysis of air parameters in the room was undertaken using geometrical model and numerical calculations conducted in DesignBuilder software. The evaluation of technical solutions for thermal comfort maintenance was conducted based on air temperature and velocity distribution in the room of industrial boiler plant in the "Installation of Thermal Treatment of Sewage Sludge" building, located in the "Group Sewage Treatment Plant" complex in Lodz, Poland.

Method description

The "Installation of Thermal Treatment of Sewage Sludge" building is located in the "Group Sewage Treatment Plant" complex of Lodz, and consists of one room of industrial boiler plant which was a simulation domain. The room analyzed is not intended for the constant presence of people. It has a cubic capacity of 12,136 m^3. There is a mechanical ventilation system in the room designed to exhaust airflow at 180,000 m^3/h, which provides approximately a 14.8 rate of air change per hour. The air exhaust is driven by 12 roof fans, located over the main heat sources. Each fan has a nominal air flow of 15,000 m^3/h and a static pressure of 120 Pa. The air is supplied through 13 air intakes, located at the height of 2.49 m above the ground floor level. The dimensions are 2,000 mm x 1,000 mm (5 pieces) and 1,000 mm x 1,000 mm (8 pieces), with movable blinds connected to actuators coupled with roof exhaust fans. In the room, there are 2 technological process lines with a maximum total thermal capacity of 8.14 MW. Each line is equipped with a fluidized-bed incinerator (furnace) with a 4.07 MW maximum total thermal capacity, flue gas recuperator, steam heat recovery boiler, multicyclone, industrial bag filter and flue-gas stack (chimney) for removing the gaseous contaminants. Since those devices generate a significant amount of heat in the room, therefore there is no need for using a heating system in the building. In this analysis, the operation of only one technological line was assumed.

The first step of carrying out numerical calculations was to make a geometrical model of the building (fig. 1), and of the room and combustion devices (fig. 2), as well as setting up boundary conditions of outdoor air temperature, devices external surface temperature and air flow rate. The geometrical model includes all main elements affecting the temperature and velocity distributions, namely all partitions with windows, air intakes and air exhaust holes for roof fans, as well as larger equipment emitting heat. For the sake of simplifying the calculations, the model does not contain the steel structure of work platforms, mechanical equipment and lower diameter pipes. The room analyzed was divided into nearly 745,000 cells by general mesh spacing of 0.60 m, and local spacing of 0.10 m near the devices. The calculations were made using k – ε turbulence model and upwind discretisation scheme [32]. The maximum dependent variable residual for the calculations was 10^{-3}, and the number of iterations was over 4,000.
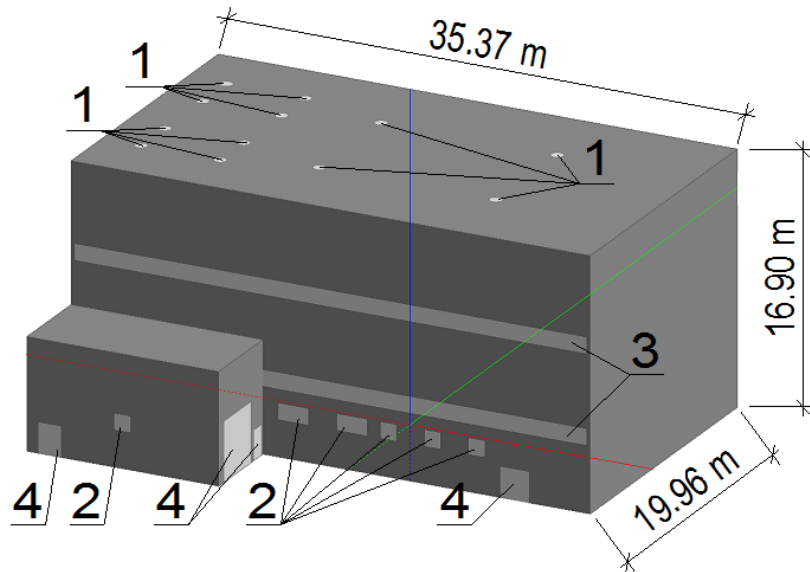
Fig. 1. Building geometrical model, where: 1 – exhaust roof fan, 2 – air intake, 3 – window, 4 - door
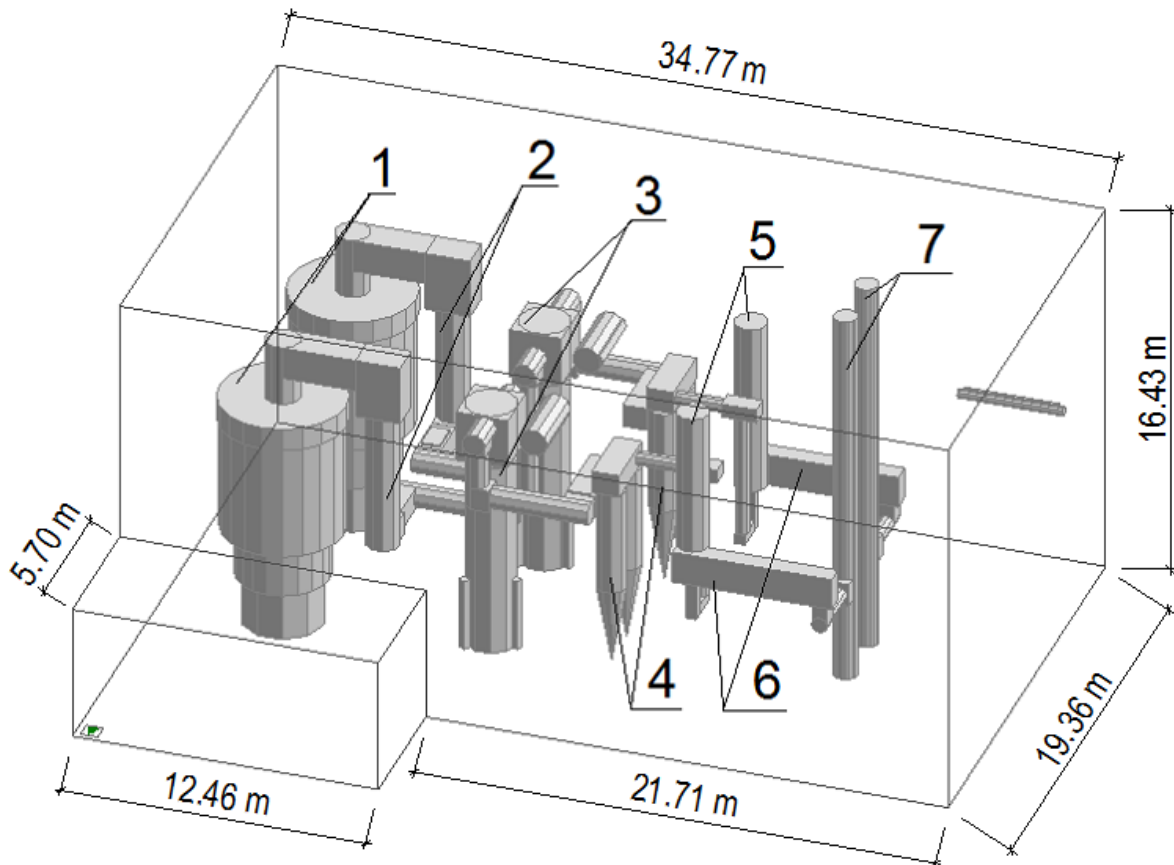*Source: Author's*

Fig. 2. Room geometrical model, where: 1 – furnace, 2 recuperator, 3 – boiler, 4 – multicyclone, 5 – steam cooling device, 6 – bag filter, 7 – chimney
Source: Author's

The boundary conditions (table 3) were set up basing on experimental measurements of device's external surface temperature, an external temperature sensor and data concerning installation of mechanical ventilation of the room. The temperature measurements of the external surface of the devices were carried out using a radiation pyrometer for each device on 1.50 m height above each subsequent working platform. The accuracy of the pyrometer was ± 1.5 K and default emissivity coefficient was 0.95. The results of the

measurements were averaged and calculated into an actual temperature using different values of emissivity coefficient of the materials examined ε. The emissivity coefficient of a surface of the devices was assumed to be 0.88 for oxidized steel and 0.28 for galvanized steel [33]. The outdoor air temperature of + 25.0 $^{\circ}$C was obtained from building automation system using an outdoor air temperature sensor located on the external wall of the building. The accuracy of the outdoor air temperature sensor was 0.22 K. The airflow for each fan and the total airflow for the room was obtained using design data that accounted for the number of operating roof fans. Each fan has a nominal air flow of 15,000 m^3/h. From the total number of twelve fans, only nine were working, while two were out of order and one was removed. In the location of removed fan, the gravitational airflow was opened. The gravitational airflow of 2,340 m^3/h was calculated using measuring results from an air velocity meter with 5% accuracy. Therefore the total ventilation airflow was 137,340 m^3/h.

Table 3. Boundary conditions for numerical calculations

Boundary condition type	Value
Outdoor air temperature	+ 25.0 $^{\circ}$C
Airflow through each fan	15,000 m^3/h
Gravitational airflow through hole	2,340 m^3/h
Total ventilation of ventilation system	137,340 m^3/h
Temperature of external surface of the furnace*	+ 55.0-117.6 $^{\circ}$C
Temperature of external surface of the recuperator*	+ 57.2-105.5 $^{\circ}$C
Temperature of external surface of the other devices*	+ 37.0-61.9 $^{\circ}$C
Temperature of external walls	+ 25.0 $^{\circ}$C
Temperature of ground floor	+ 20.0 $^{\circ}$C
* The devices were divided into parts of different measured temperatures of external surface, wherein the raise of the temperature occurs along with increase of height	

Source: Author's

The room analyzed has 8 levels of work area with the following floor heights and work platforms: ± 0.00 m, + 2.75 m, + 4.00 m, + 5.30 m, + 7.05 m, + 7.90 m, + 9.30 m and + 11.60 m. Because most work is done standing, the temperature and velocity of air was calculated on the height of head of the worker, which is 1.70 m above the floor level. In this article, the air parameters were analyzed on a sample of two heights (+ 1.70 m and + 11.00 m) from work areas and places where equipment maintenance takes place.

The outdoor air temperature was obtained using indication of temperature sensor located on the building wall. An impact of solar radiation and wind on indoor air conditions was omitted due to crucial influence of ventilation system and heat generated by combustion plant. The temperature of walls was assumed as 25.0°C, and the temperature of ground floor as 20.0°C. The temperature of supply air was set to 25.0°C. The validity of the simulation was assured using experimental measurements of air temperature in five points of the room on different heights from + 1.10 m to + 12.70 m. The measurements of air temperature were made using LSI LASTEM BSU102 psychrometer probe [34] with ± 0.19 K accuracy.

Results

The verification of the simulation, comparing measured and CFD calculated air temperature in the room analyzed, showed an average comparison error of 6.4 % with CFD results overestimation at the lower parts of the rooms, and underestimation at the upper levels. The results of the numerical analysis were presented using the distribution of the air temperature and velocity. On the level of + 1.70 m, corresponding to height of head of employee, there was a rise in the ambient temperature from + 24.0°C near a non-operational process line + 25.2°C at a distance of 1.0 m from the furnace and other devices generating heat (fig. 3). A slight ambient

temperature increase is associated with the lower temperature of the devices in their lower parts. The analysis of the air temperature distribution shows that at the level of +1.70 m, thermal comfort requirement are fulfilled in approximately 90% of the area according to comfort category C during summer, which is specified in the ISO 7730:2005 standard [11]. A radiant asymmetry is not a concern in this case. An impact of hot surfaces of the devices on the thermal comfort can be assumed to be similar to an impact of a hot wall surface, which does not exceed 10% PPD [11]. This situation concerns the radiant asymmetry lower than 35°C. The ISO 7730:2005 standard [11] does not provide information on the impact of higher radiant asymmetry values on the thermal comfort.
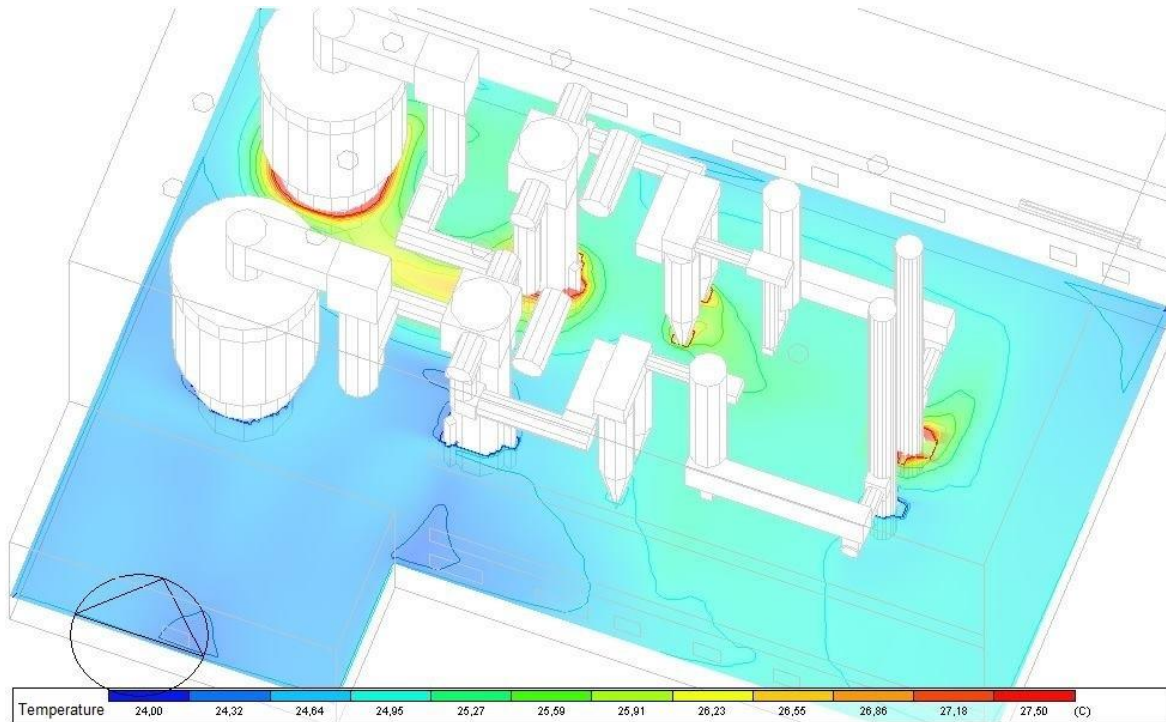

| Temperature | 24,00 | 24,32 | 24,64 | 24,95 | 25,27 | 25,59 | 25,91 | 26,23 | 26,55 | 26,86 | 27,18 | 27,50 | (C) |

Fig. 3. Air temperature distribution on the level of + 1.70 m
Source: Author's

The analysis of the distribution of air velocity at the level of + 1.70 m shows significant changes of its value, from 0.00 m/s in the corners of the rooms, to 0.64 m/s in the vicinity of the operating process line, and above 1.00 m/s near the boiler and multicyclone (fig. 4). Those high values were associated with the location of air intakes at the level of +2.49 m, so the influence of the supply stream on the air conditions is noticeable in the analyzed area, where dominated speeds above 0.50 m/s predominated. The velocity comfort requirements during the summer were not fulfilled, as specified in the ISO 7730:2005 standard [11], because the air velocity should not exceed 0.23 m/s (table 2) in the work area.
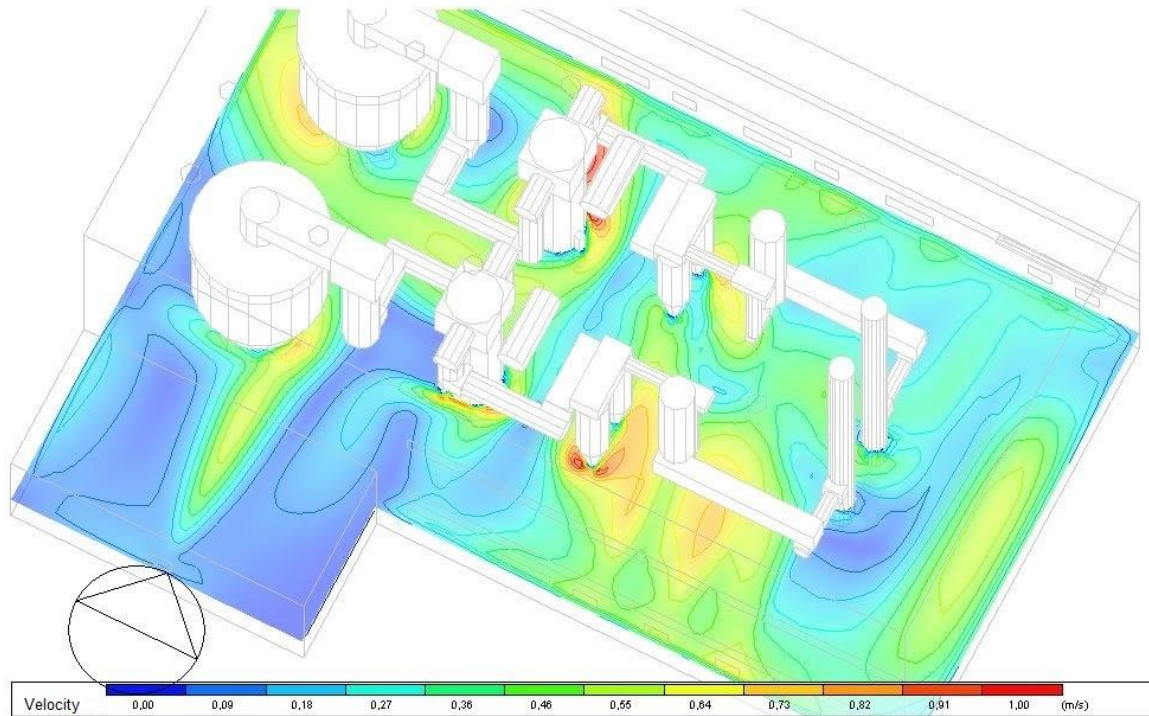
Fig. 4. Air velocity distribution on the level of + 1.70 m
Source: Author's

At the level of + 11.00 m, which is the height of head of an employee while maintaining the devices on the 7th level of the work platform, it was a significant temperature rise, especially near the furnace, boiler and multicyclone (fig. 5). The temperature in the case analyzed varied from + 26.0 $^{\circ}$C to + 32.0 $^{\circ}$C at a distance of 1.0 m from the furnace to + 35.0 $^{\circ}$C at a distance of 0.5 m from its rear section. The increase of air temperature near the heat sources is caused by the operation of mechanical ventilation lifting the heated air along the entire height of the devices. The major area has a temperature around +27.1 $^{\circ}$C, which does not fulfill the thermal comfort requirements during summer, as specified in the standard of ISO 7730:2005 [11], because the air temperature should not exceed 26°C (table 2) in the work area.
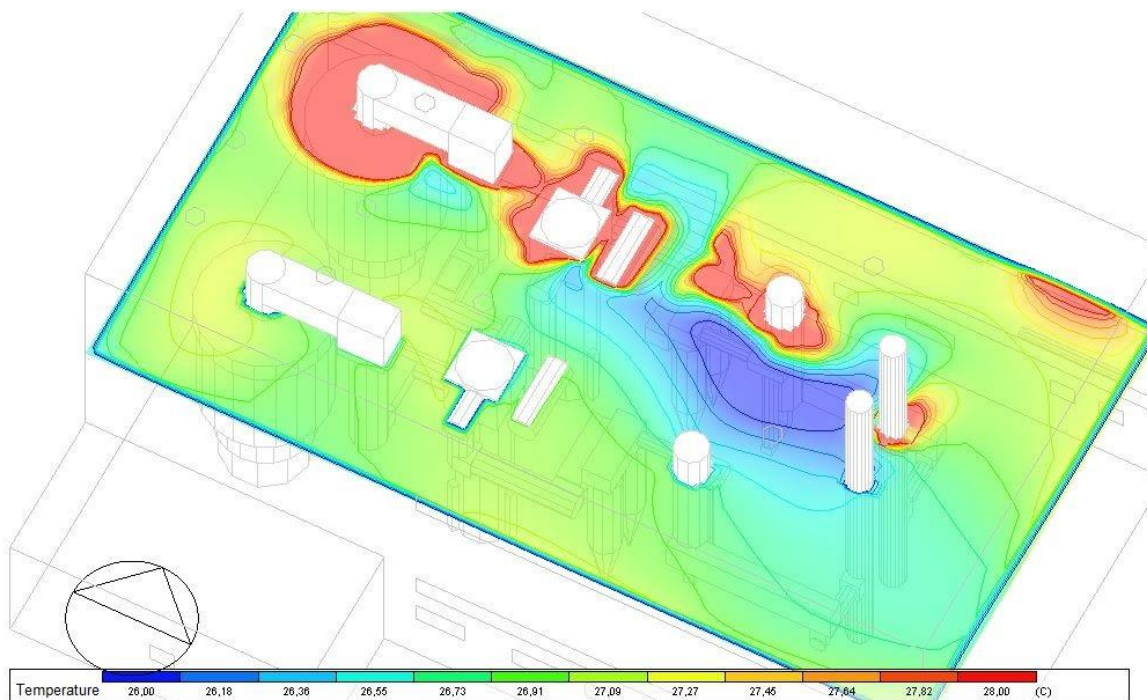

Fig. 5. Air temperature distribution on level of + 11.00 m
Source: Author's

The analysis of air velocity distribution at the level of + 11.00 m showed lower variations than at the level of + 1.70 m. While on the lower level the air velocity is above 0.30 m/s in approximately 60% of the area, on upper level this value is exceeded only near the furnace, boiler and steam cooling devices. However, both levels showed similarly low air velocities (approximately 0.00 m/s) in the building corners and increased to 1.00 m/s near the operating technological line, where the velocity is in the range of 0.15-0.20 m/s (fig. 6), which fulfills category B requirements for velocity comfort during summer according to the ISO 7730:2005 standard [11].
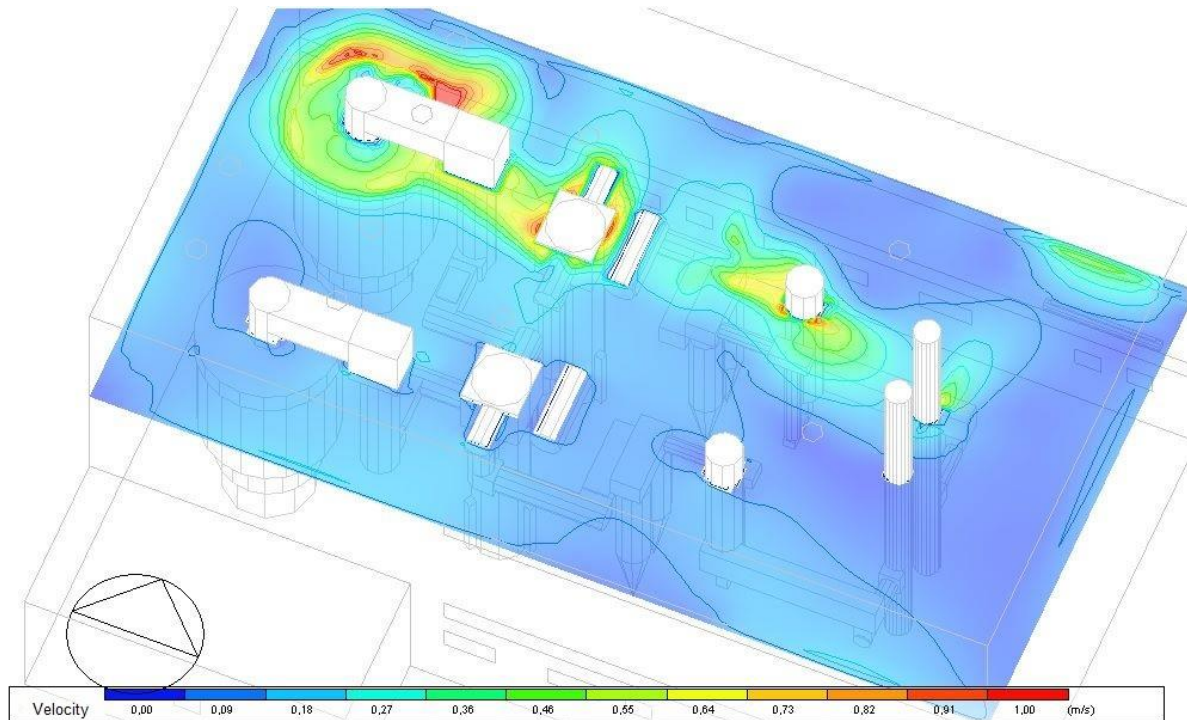

Fig. 6. Air velocity distribution on the level of + 11.00 m
Source: Author's

From the analysis carried out, it follows that the air temperature varied from + 23.5 °C near the non-operational process line to + 35.0 °C near the furnace, and the air velocities varied up to 1.0 m/s. The numerical analysis showed that at the + 1.70 m level, the comfort requirements for temperature were fulfilled in approximately 90% of the area. However, recommended air velocities were exceeded in approximately 80% of the area. A reverse phenomenon was noticed at +11.00 m, where the air velocity requirements were fulfilled in contrast to temperature requirements. Additionally, in the middle of the boilers (approximately 2.5 m distance) the air temperature at + 1.70 m was to + 25.3 °C with a velocity of 0.56 m/s, while at + 11.00 m it reached to + 27.0 °C with a velocity of 0.19 m/s. There was a threefold decrease of velocity, and a 0.57% increase of absolute temperature in this specific cross-section. Although the temperature rise seems small, it is sufficient to exceed the recommended values for light activity, indicating significant differences in the thermal comfort of people operating and maintaining combustion devices. It also shows the effectiveness of the removal of heat gains generated during the operation of combustion plant equipment, which was indicated by high air velocity (approximately 1.0 m/s) near the heat sources associated with process of hot air convection and by rapid drop in temperature. One meter away from those devices, the air temperature decreased to + 32 °C, down from + 117.6 °C at the external surface of the furnace.

In the room analyzed, the temperature rises along with height which indicates implementation of stratification strategy [9, 35] by ventilation system. However, the air is supplied on the bottom of the room at a high speed, which is characteristic for mixing strategy [9, 36] that assumes providing a uniform distribution of heat and contaminants throughout the ventilated space. The optimum solution of the industrial ventilation operation is to reach the lowest possible ratio of temperature in working zone to the temperature of air flowing from the room [9, 37], which was partly reached in the room analyzed. The comfort requirements in terms of temperature criterion are not fulfilled because the work platforms are located at a high level.

Conclusions

The numerical analysis of air parameters in a room equipped with combustion devices indicates that thermal comfort requirements for workers conducting light activity from a standing position are not fulfilled, according to the ISO 7730:2005 [11] standard.

It was also found that the recommended air velocity was exceeded at +1.70 m, and the recommended air temperature at +11.00 m, which can cause negative thermal sensations of room's microclimate. The analysis of the air temperature and velocity indicated that the operation of mechanical ventilation, supported by convection streams of air heated from combustion devices, allows a significant removal of heat gains associated with thermal emission during the operation of combustion plant equipment. However, this solution does not meet the requirements of thermal comfort of workers in most working areas, especially when the outdoor air temperature is high and there are heat-generating devices in proximity. What is more, it is necessary to take under consideration that analysis was undertaken with condition of only one working technological line and in the case of operation of both process lines, the heat gains would increase. As a result, there would be an increase of ambient temperature and a worsening of thermal comfort conditions.

Meeting the workers' thermal comfort requirements needs an effective solution for heat gain removal and lower air supply velocities. Since the rating of local microclimate decreases with the rise of air temperature and velocity, the thermal comfort sensation goes down as one approaches combustion devices. Improvement of thermal comfort in the room analyzed can be achieved increasing thermal insulation of combustion devices and performing local exhaust ventilation extracting the hot air directly above them. This will prevent spreading the heat into the room. Applying local ventilation cooperating with general ventilation system facilitates better thermal conditions in a work zone, resulting from the reduction of heat gains and contaminants while simultaneously supplying fresh air [1]. Hermetization of the heat processes will probably effect in drop of the ventilation airflow, causing the reduction of velocities of the supply air, and consequently of the air velocities in the lower parts of the room. Decrease of the supply air velocities can also be obtained enlarging dimensions of the air intakes.

Providing thermal comfort in rooms not equipped with air-conditioning system become very problematic when outdoor air conditions cause a heat discomfort [15]. In the case analyzed, when workers are conducting light industry activity, the thermal requirements in the room will not be met for the air supply temperature over 26°C (table 2). Therefore, there is a need for operation of an air-conditioning system during the summer to maintain a thermal comfort in the industrial rooms.

The effectiveness of industrial ventilation is determined by the proper distribution of air and the knowledge about the amount of generated contaminants, heat and location of their sources [8]. The CFD analysis methods facilitate the optimization of technical solutions at the stage of industrial ventilation system design, as well as a verification of effectiveness of its operation [38].

References

[1] A. Charkowska, Wymagania ogólne i podstawowe zasady projektowania wentylacji dla obiektów przemysłowych (General requirements and basic rules of ventilation system design in industrial buildings), Special supplement IB – Ventilation and air-conditioning, Inżynier Budownictwa (Civil Engineer) 10 (2013) 62-64.

[2] R. Cichowicz, G. Wielgosiński, A. Targaszewska, Analysis of CO2 concentration distribution inside and outside small boiler plants, ECOL CHEM ENG S. 23 (1) (2016) 49-60, DOI: 10.1515/eces-2016-0003.

[3] R. Cichowicz, G. Wielgosiński, Effect of meteorological conditions and building location on CO_2 concentration in the university campus, ECOL CHEM ENG S. 22 (4) (2015) 513-525, DOI: 10.1515/eces-2015-0030.

[4] J. Szymańska, Podstawy wentylacji przemysłowej (Basics of industrial ventilation), Magazyn Przemysłowy (Industrial Magazine) 2016.

[5] D. Węgrzyn, Powietrze dla przemysłu (Air for industry), Magazyn Instalatora (Plumber Magazine) 12 (2012) 12-14.

[6] R. Rota, Industrial Ventilation, Ref. Mod. in Chem., Mol. Sc. and Chem. Eng. (2015), DOI: 10.1016/B978-0-12-409547-2.11223-5.

[7] A. Mabbett, Industrial ventilation and air pollution control, Metal Finishing 105 (10) (2007) 678-698, DOI: 10.1016/S0026-0576(07)80385-0.

[8] D. Węgrzyn, Wentylacja przemysłowa (Industrial Ventilation), Magazyn Instalatora (Plumber Magazine) 4 (2012) 16-17.

[9] B. Biegert, J. Railio, Terminology, in: H. Goodfellow, E. Tahti (Eds.), Industrial Ventilation. Design Guidebook, Academic Press, 2001, pp. 9-14.

[10] I. Sudoł-Szopińska, A. Chojnacka, Określanie warunków komfortu termicznego w pomieszczeniach za pomocą wskaźników PMV i PPD (Determining thermal comfort conditions in rooms with the PMV and PPD indices), Bezpieczeństwo Pracy (Occupational Safety) 5 (2007) 19-23.

[11] ISO 7730:2005 Ergonomics of the thermal environment - Analytical determination and interpretation of thermal comfort using calculation of the PMV and PPD indices and local thermal comfort criteria.

[12] G. Havenith, Heat balance when wearing protective clothing, ANN OCCUP HYG 43 (5) (1999) 289-296, DOI: 10.1016/S0003-4878(99)00051-4.

[13] T. Fukazawa, G. Havenith, Differences in comfort perception in relation to local and whole body skin wittedness, Eur. J. Appl. Physiol. 106 (1) (2009) 15-24, DOI: 10.1007/s00421-009-0983-z.

[14] ISO 7243:1989 Hot environments – Estimation of the heat stress on working man, based on the WGBT-index (wet bulb globe temperature).

[15] N. M. Pinto, A. A. P. Xavier, K. Hatakeyama, Thermal comfort in industrial environment: conditions and parameters, Procedia Manufacturing 3 (2015) 4999 – 5006, DOI:10.1016/j.promfg.2015.07.662.

[16] L. Lan, Z. Lian, Y.Liu, Investigation of gender difference in thermal comfort for Chinese people, Eur. J. Appl. Physiol. 102 (4) (2008) 471-480, DOI: 10.1007/s00421-007-0609-2.

[17] D. Skrzyniowska, Parameters of indoor air in residential and non-residential buildings. Thermal Comfort, Technical Transactions. Environmental Engineering 4 (2012) 15-35.

[18] A. Auliciems, S. V. Szokolay, Thermal comfort, PLEA in association with Dept. of Architecture, University of Queensland, 2007.

[19] J. B. Joshi, Computational Fluid Dynamics for Designing Process Equipment: Expectations, Current Status and Path Forward, Ind. Eng. Chem. Res. 42 (6) (2003) 115-1128, DOI: 10.1021/ie0206608.

[20] S. Yang, X. Li, C. Yang, B. Ma, Z. Mao, Computational Fluid Dynamics Simulation and Experimental Measurement of Gas and Solid Holdup Distribution in a Gas-Liquid-Solid Stirred Reactor, Ind. Eng. Chem. Res. 55 (12) (2016) 3276-3286, DOI: 10.1021/acs.iecr.5b03163.

[21] K. S. Nikas, N. Nikolopoulos, A. Nikolopoulos, Numerical study of a naturally cross-ventilated building, Energy and Buildings 42 (4) (2010) 422-434, DOI: 10.1016/j.enbuild.2009.10.010.

[22] Y. Ji, M.J. Cook, V. Hanby, CFD modelling of natural displacement ventilation in an enclosure connected to an atrium, Building and Environment, 42 (3) (2007) 1158-1172, DOI: 10.1016/j.buildenv.2005.11.002.

[23] http://www.openfoam.com

[24] http://www.ansys.com/Products/Fluids/ANSYS-Fluent

[25] http://www.thunderheadeng.com/pyrosim

[26] https://www.designbuilder.co.uk

[27] A. Bohojło, M. Kołodziejczyk, Computational analysis of local thermal comfort factors in a habitatle room, Acta mechanica et automatic 3 (1) (2010) 14-23.

[28] R. Cichowicz, A. Lewandowska, The analysis of selected parameters of thermal comfort in the classrooms using CFD techniques, WSN 73 (1) (2017) 72-79.

[29] M. Manickam, M. P. Schwarz, J. Perry, CFD modeling of waste heat recovery boiler, Applied Mathematical Modelling 22 (10) (1998) 823-840, DOI: 10.1016/S0307-904X(98)10020-3.

[30] H. Chen, Z. Liang, Damper opening optimization and performance of a co-firing boiler in a 300 MWe plant, Applied Thermal Engineering 123 (2017), DOI: 10.1016/j.applthermaleng.2017.05.085.

[31] R. Rota, L. Canossa, G. Nano, Ventilation design of industrial premises through CFD modeling, CAN J CHEM ENG 79 (1) (2001), DOI: 10.1002/cjce.5450790112.

[32] Technical CFD Documentation. DesignBuilder Software, http://www.designbuilder.co.uk/downloads/CFDTechnical.pdf

[33] T. Hobler, Heat transfer and heat exchangers (Ruch ciepła i wymienniki), Państwowe Wydawnictwo Techniczne (National Technical Publishing), Warsaw, 1959

[34] Microclimatic probes. User's manual, LSI LASTEM, http://www.lsi-lastem.it/WebDocument/INSTUM_00499_it-en.pdf

[35] Y. J. P. Lin, J. Y. Wu, A study on density stratification by mechanical extraction displacement ventilation, INT J HEAT MASS TRAN 110 (2017) 447-459, DOI: 10.1016/j.ijheatmasstransfer.2017.03.053.

[36] A. C. Caputo, P. M. Pelagagge, Upgrading mixed ventilation systems in industrial conditioning, Applied Thermal Engineering 29 (14-15) (2009) 3204-3211, DOI: 10.1016/j.applthermaleng.2009.04.025.

[37] S. Mierzwiński, Wentylacja Przemysłowa. Cz. I (Industrial Ventilation. Vol. I), Silesian University of Technology, Gliwice, 1979

[38] B. Biegert, J. Railio, Industrial Air Technology - Description, in: Goodfellow H., Tahti E. (Eds.), Industrial Ventilation. Design Guidebook, Academic Press, 2001, pp. 1-7